

Global Biogeochemical Cycles®



RESEARCH ARTICLE

10.1029/2021GB007115

Biogeochemical Dynamics in Adjacent Mesoscale Eddies of Opposite Polarity

Key Points:

- The steepness of the nutricline in mature mesoscale eddies is an important driver of variability in pelagic ecosystems
- Differences in eukaryotic phytoplankton communities alter the export of particulate inorganic carbon and particulate silica across eddies
- Relative changes in oxygen and nutrients linked to displacements of the thermocline reflect anomalous cycling of organic matter

Supporting Information:

Supporting Information may be found in the online version of this article.

Correspondence to:

B. Barone and M. J. Church,
benedetto.barone@gmail.com;
matt.church@flbs.umt.edu

Citation:

Barone, B., Church, M. J., Dugenne, M., Hawco, N. J., Jahn, O., White, A. E., et al. (2022). Biogeochemical dynamics in adjacent mesoscale eddies of opposite polarity. *Global Biogeochemical Cycles*, 36, e2021GB007115. <https://doi.org/10.1029/2021GB007115>

Received 2 JUL 2021

Accepted 10 JAN 2022

Author Contributions:

Conceptualization: Benedetto Barone, Matthew J. Church, Edward F. DeLong, David M. Karl











Data curation: Mathilde Dugenne, Nicholas J. Hawco, Oliver Jahn

Formal analysis: Benedetto Barone, Matthew J. Church, Mathilde Dugenne, Nicholas J. Hawco

Funding acquisition: Matthew J. Church, Angelique E. White, Seth G. John, Michael J. Follows, Edward F. DeLong, David M. Karl

© 2022. The Authors.

This is an open access article under the terms of the [Creative Commons Attribution License](https://creativecommons.org/licenses/by/4.0/), which permits use, distribution and reproduction in any medium, provided the original work is properly cited.

Benedetto Barone^{1,2} , **Matthew J. Church**³ , **Mathilde Dugenne**^{1,2} , **Nicholas J. Hawco**^{2,4} , **Oliver Jahn**⁵ , **Angelique E. White**^{1,2} , **Seth G. John**⁴ , **Michael J. Follows**⁵ , **Edward F. DeLong**^{1,2} , and **David M. Karl**^{1,2} 

¹Daniel K. Inouye Center for Microbial Oceanography: Research and Education, University of Hawai'i at Mānoa, Honolulu, HI, USA, ²Department of Oceanography, University of Hawai'i at Mānoa, Honolulu, HI, USA, ³Flathead Lake Biological Station, University of Montana, Polson, MT, USA, ⁴Department of Earth Sciences, University of Southern California, Los Angeles, CA, USA, ⁵Department of Earth, Atmospheric and Planetary Sciences, Massachusetts Institute of Technology, Cambridge, MA, USA

Abstract We examined the biogeochemical impact of paired mesoscale cyclones and anticyclones in spatial proximity (<200 km apart) in the North Pacific Subtropical Gyre. While previous studies have demonstrated that upwelling associated with the intensification of cyclonic eddies can supply nutrients supporting plankton productivity, we observed that steeper vertical gradients in inorganic nutrients increased nutrient fluxes due to diapycnal mixing during the mature stage of cyclonic eddies. The increased diapycnal nutrient supply was linked with expansion of eukaryotic phytoplankton biomass and intensification of the deep chlorophyll maximum (DCM) layer. This perturbation in the plankton community was associated with increased fluxes of biominerals (specifically particulate inorganic carbon and particulate silica) and isotopically enriched organic nitrogen in particles exported in the cyclone. The time-integrated effects of thermocline vertical displacements on the lower euphotic zone were predictable deficits and surpluses of inorganic nutrients and dissolved oxygen, respectively. However, the stoichiometry of oxygen and inorganic nutrients differed from that predicted for production and consumption of phytoplankton biomass, requiring additional biological processes that decouple changes in oxygen and nutrient concentrations. The dynamics revealed by this study may be a common feature of oligotrophic ecosystems, where mesoscale biogeochemical perturbations are buffered by the DCM layer, which limits the ecological impact of eddies in the well-lit, near-surface ocean.

1. Introduction

Subtropical gyres are the dominant circulation features in all major ocean basins, enclosing large biomes that cover ~40% of the Earth's surface (McClain et al., 2004; Pedlosky, 1990). Ecological variability in the subtropical gyres is closely linked to physical variability driven by ocean currents, which are most energetic at the mesoscale (10–100's of km) where the circulation forms closed vortices called nonlinear mesoscale eddies (Chelton et al., 2007; Mackas et al., 1985; Munk, 2002). A prior study, from a fixed location in the North Pacific Subtropical Gyre (NPSG), revealed eddies were present 30% of the time (Barone et al., 2019). Hence, understanding how mesoscale eddies impact pelagic ecosystem functioning in subtropical gyres is an important step to identify the main drivers of biogeochemical variability in these expansive biomes.

Eddies exert direct influence on plankton biogeochemistry through vertical oscillations of the thermocline, with concomitant changes in the distributions of nutrients relative to the upper ocean light field (Falkowski et al., 1991; Wunsch, 1997). Cyclonic eddy uplift of the thermocline can enhance the supply of inorganic nutrients to the euphotic zone, while downward displacement of the thermocline in anticyclonic eddies can move the deep reservoir of inorganic nutrients further away from the sunlit upper ocean (McGillicuddy & Robinson, 1997; Venrick, 1990). Cyclonic eddies undergo time-variable physical and biological responses to the active upwelling of inorganic nutrients to the euphotic zone, which supports periods of elevated phytoplankton production (Rii et al., 2008; Sweeney et al., 2003). Nutrient upwelling can also result from eddy/wind interactions in mode-water eddies, which similarly stimulates phytoplankton growth in the euphotic zone (McGillicuddy et al., 2007).

Satellite remote sensing has previously been leveraged to describe the impact of mesoscale eddies on near-surface ocean plankton dynamics by analyzing spatial anomalies in chlorophyll concentrations relative to the eddy field (Chelton et al., 2011; Gaube et al., 2014; Guo et al., 2019). These mesoscale chlorophyll anomalies are caused

Investigation: Benedetto Barone, Matthew J. Church, Mathilde Dugenne, Nicholas J. Hawco, Angelicque E. White, Seth G. John, Michael J. Follows, David M. Karl

Methodology: Benedetto Barone, Matthew J. Church, Mathilde Dugenne, Nicholas J. Hawco, Angelicque E. White, Michael J. Follows, David M. Karl

Resources: Matthew J. Church, Angelicque E. White, Seth G. John, Michael J. Follows, Edward F. DeLong, David M. Karl

Software: Oliver Jahn, Michael J. Follows

Supervision: David M. Karl

Visualization: Benedetto Barone, Matthew J. Church

Writing – original draft: Benedetto Barone, Matthew J. Church

Writing – review & editing: Benedetto Barone, Matthew J. Church, Mathilde Dugenne, Nicholas J. Hawco, Oliver Jahn, Angelicque E. White, Seth G. John, Michael J. Follows, Edward F. DeLong, David M. Karl

by different processes including horizontal stirring, vertical motions, and trapping and transport of water parcels, with different processes driving the variability in different oceanic regions (Gaubert et al., 2014; Guo et al., 2019). While satellite-based approaches provide valuable insights into physical-biological interactions associated with eddies, in the open ocean they are typically restricted to depths <25 m (first optical depth; Gordon & McCluney, 1975) and do not provide information on dynamics occurring in the deeper regions of the euphotic zone. This is particularly important in stratified ecosystems where the surface mixed layer tends to be much shallower than the euphotic zone, and phytoplankton dynamics occurring within vertically distinct layers of the upper ocean can be decoupled.

In this study, we focused on mesoscale eddies in the permanently stratified central NPSG. This ecosystem is characterized by persistently low inorganic nutrients throughout the upper ~100 m, where there is sufficient light to drive net primary production (Karl, 1999). In this environment, phytoplankton communities are vertically segregated, with populations in the near-surface waters distinct from those in the lower portion of the euphotic zone, between 100 and 175 m depth (Malmstrom et al., 2010; Venrick, 1982, 1999). Low-light adapted phytoplankton assemblages inhabit the deep chlorophyll maximum (DCM), a persistent feature in stratified ocean ecosystems (Li et al., 2011; Malmstrom et al., 2010). The DCM is vertically associated with the top of the nitracline, here defined as the layer where inorganic nitrogen concentrations start increasing with depth, and where turbulent mixing provides an upward flux of inorganic nitrogen to the euphotic zone (Anderson, 1969; Bahamón et al., 2003; Cullen & Eppley, 1981; Herbland & Voituriez, 1979; Lewis et al., 1986). In the NPSG, the vertical position of the DCM is defined by time-varying changes in the depth of light penetration, and this feature broadly marks the transition between nutrient-limited phytoplankton growth above it and light-limited phytoplankton growth below it (Cullen, 2015; Letelier et al., 2004). Increased light energy to the lower euphotic zone during the summer months allows vertical expansion of the upper ocean habitat available to phytoplankton, resulting in a downward vertical displacement of the DCM into denser, more nutrient-enriched waters (Letelier et al., 2004). In an analogous way, through changes in the depth of isopycnal surfaces across an exponential attenuation in light flux, mesoscale dynamics structure the vertical positioning of the DCM phytoplankton community, with the DCM forming along colder, denser waters during periods of isopycnal uplift, such as those driven by cyclonic eddies (Falkowski et al., 1991; Kuwahara et al., 2008; Letelier et al., 2000; McGillicuddy et al., 1999; Vaillancourt et al., 2003).

The main objective of this research was to better define the impacts that mesoscale eddies have on the near-surface and DCM plankton communities. To do so, we sampled adjacent eddies with opposite polarity, cyclonic and anticyclonic, in close spatial proximity, during two research cruises conducted in 2016 and 2017. Studying adjacent eddies permitted direct comparison of these features without complications due to larger-scale horizontal variability. The eddies sampled as part of these cruises represented extreme mesoscale events for this region, providing new information on biogeochemical and plankton dynamics associated with strong mesoscale perturbations (Barone et al., 2019). The generality of the biogeochemical and ecological responses observed in these strong eddies was subsequently evaluated by leveraging the Eulerian observations of the Hawaii Ocean Time-series (HOT) program (Karl & Lukas, 1996).

2. Material and Methods

2.1. Identification of Eddies

We sampled adjacent eddies of opposite polarity during two oceanographic expeditions: Hawaii Ocean Experiment (HOE)-Legacy 4 (HL4) aboard the R/V Ka'imikai-O-Kanaloa (May 9–14, 2016); and Microbial Ecology of the Surface Ocean—Simons Collaboration on Ocean Processes and Ecology (MESO-SCOPE) aboard the R/V *Kilo Moana* (26 June–15 July 2017). Eddies were identified as minima (cyclones) and maxima (anticyclones) in sea level anomaly (SLA) based on a combination of altimetry from all available satellites distributed by the Copernicus Marine Environment Monitoring Service (<http://marine.copernicus.eu/>). The SLA product was corrected for interannual trend and seasonal cycle following procedures recently proposed for the nearby Station ALOHA (A Long-term Oligotrophic Habitat Assessment), located at 22°45' N and 158°W; the resulting corrected SLA is henceforth termed SLA_{corr} (Barone et al., 2019).

Prior to each cruise, maxima and minima in SLA_{corr} in waters north of the Hawaiian Islands were monitored for several weeks; the selection of eddies to sample for these cruises included consideration of proximity to Station ALOHA (for historical context and logistical considerations), the strength of the adjacent eddies (based

on SLA_{corr}), and assessment of time-varying eddy behavior (e.g., strengthening or weakening in SLA_{corr}). Eddy coordinates, age, and amplitude were tracked in time using a simple algorithm: For each daily map of SLA_{corr} , the eddy center was defined as the minimum or maximum of SLA_{corr} in a square with a side of 1.5° centered on the coordinates of the eddy center on the previous day. The amplitude of an eddy was defined as the value of SLA_{corr} at the minimum or maximum. The age of each eddy was defined as the number of days since the time of first detection, which was subjectively assessed as the first day when a minimum or maximum detached from a larger area of positive or negative SLA_{corr} . Similarly, the last day of eddy detection was subjectively defined as the day when a minimum or maximum of SLA_{corr} could no longer be distinguished within a larger region with positive or negative SLA_{corr} .

While we adopted a simplified tracking algorithm to describe eddy life history, eddies are also routinely cataloged and tracked within the altimetric Mesoscale Eddy Trajectories Atlas (META2.0) distributed by AVISO+ (Archiving, Validation and Interpretation of Satellite Ocean data; Schlax & Chelton, 2016). The four eddies sampled in this study were all reported in the eddy atlas, but the MESO-SCOPE cyclone was considered as a single feature together with a second cyclonic eddy during part of its lifetime. However, the trajectory of the surface drifters (described in Section 2.5) deployed during MESO-SCOPE showed cyclonic circulation around the SLA_{corr} minimum defined as the eddy center in this study; hence it is likely that the two minima which were merged in the eddy atlas represented distinct features.

2.2. Water Sampling and Profiling Instruments

During transit, the hydrographic characteristics were measured using underway conductivity, temperature, and depth (CTD) profilers (underway CTD, Teledyne), while current speed and direction were measured using a hull-mounted acoustic doppler current profiler (ADCP, Workhorse 300 kHz, Teledyne). Upper ocean biogeochemical properties were characterized using a rosette system mounting 10 L Niskin® sampling bottles and profiling instruments including a CTD sensor (Sea-Bird 911 plus), a chlorophyll fluorometer (Seapoint SCF), a polarographic oxygen (O_2) sensor (SBE 43, Sea-Bird), and a transmissometer (c-star, Sea-Bird). In situ chlorophyll fluorescence was calibrated using a linear regression against the concentration of chloropigments (comprised mostly of monovinyl and divinyl forms of chlorophyll a and b), measured fluorometrically. Similarly, the O_2 sensor was calibrated from a linear regression of dissolved O_2 concentrations determined at discrete depths measured using a Winkler titration system (see below). Beam attenuation measurements that exceeded three standard deviations from the mean (based on 20 m vertical bins) were removed in order to exclude observations presumably due to rare, large particles. Furthermore, to account for variations in sensor background values among deployments, the minimum value measured between 350 and 400 m was subtracted from each beam attenuation profile (this approach assumes that particle scattering is constant in the 350–400 m layer).

Light flux at discrete depths was calculated as the product of the daily-integrated downwelling cosine PAR irradiance above the sea surface measured with a shipboard sensor (LI-COR LI-190), and the fraction of downwelling PAR penetrating at depth measured using a free-falling optical profiler (Sea-Bird Hyperpro II). The average depth sampled for all vertical profiles was 161 ± 25 m (\pm standard deviation). Light penetration below the maximum depth was assessed by extrapolating the exponential decrease of light measured in the deepest 25 m of each vertical profile.

2.3. Eddy Transects

Physical and biogeochemical characterizations of each of the eddy couples were obtained by shipboard sampling along an approximately linear transect crossing both eddy centers (Figures 1a and 1b). An initial physical characterization was obtained while transiting using the ADCP and the underway CTD. Biogeochemical observations were obtained at a lower horizontal resolution along transects including five stations in 2016 and eleven stations in 2017, where samples were collected using the CTD rosette sampler. For these stations, hydrography and other profiling sensor observations were measured using the instruments attached to the CTD rosette.

During HL4 (in 2016) there was a failure of the conductivity sensor that prevented an accurate determination of salinity; hence, for this cruise only temperature observations from the underway CTD are presented. Since this problem only impacted the underway instrument, measurements of salinity and potential density associated

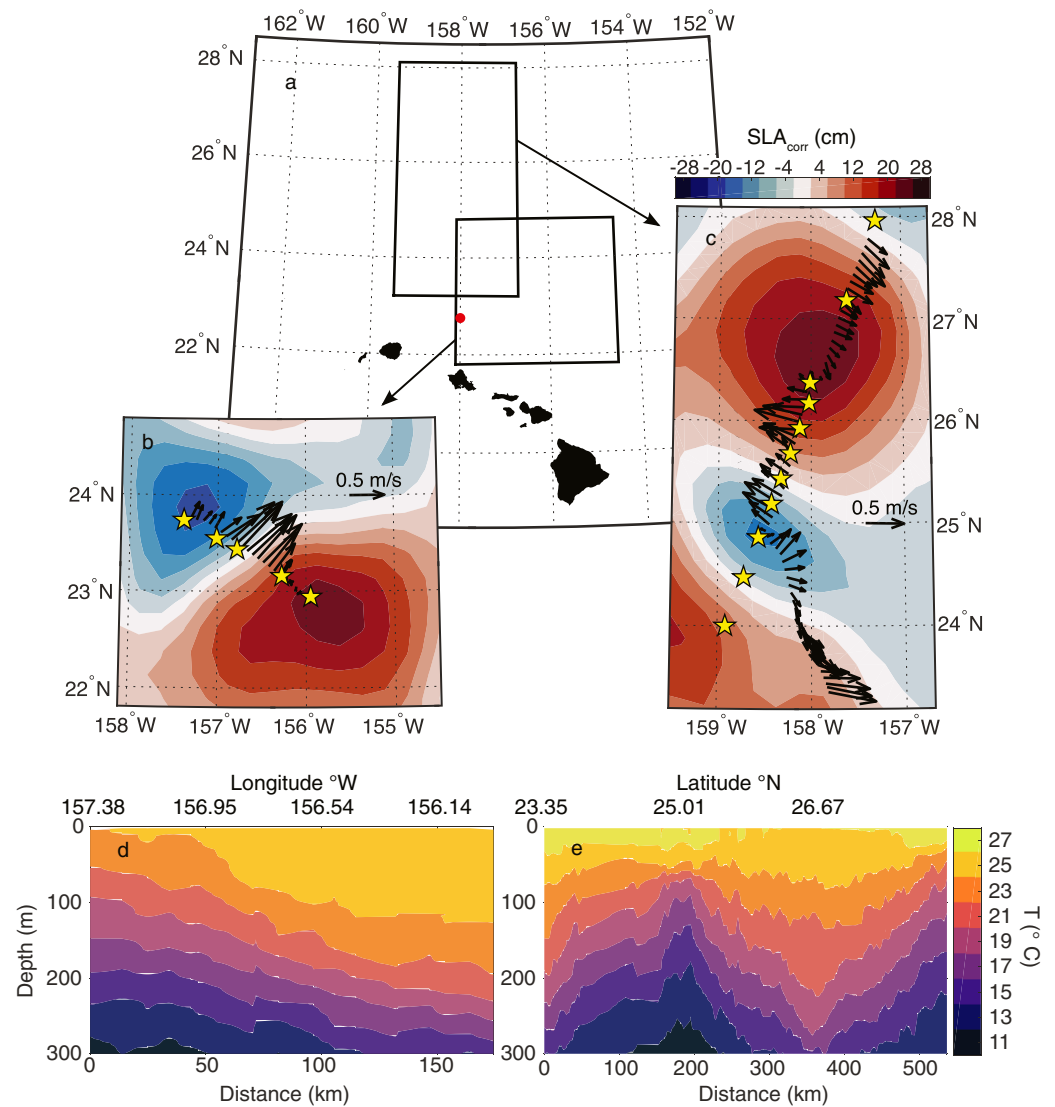


Figure 1. Sampling across adjacent mesoscale eddies during the two expeditions described in this study. The ocean near the Hawaiian archipelago is depicted in (a) with black boxes representing the regions sampled during HL4 and MESO-SCOPE, and the red circle representing the position of Station ALOHA. Contours of sea level anomaly are depicted in (b) during HL4 (11 May 2016), and (c) MESO-SCOPE (28 June 2017). Arrows depict the average current velocity and direction measured from the research vessel with an acoustic doppler current profiler in the 11–61 m depth layer; yellow stars depict the sampling stations along a transect where water samples were collected from the ship. Temperature contours along the transects are shown in (d) for HL4, and (e) for MESO-SCOPE. Data from 2016 include shipboard measurements as well as measurements collected with an underway profiling conductivity, temperature, and depth (CTD) system. Data from 2017 include only measurements collected with an underway CTD.

with the biogeochemical observations were still available from CTD measurements collected when the ship was stationary.

2.4. High Vertical Resolution Sampling

In the four eddy centers, the layer surrounding the DCM was characterized using high vertical resolution sampling (approximately 5 m vertical intervals) at 15 discrete depths around the DCM (six depths above the DCM, eight depths below the DCM, in addition to the DCM). The DCM was identified during each CTD deployment as the depth of the fluorescence maximum (ranging from 96 to 151 m). This sampling was consistently done at 0700 local time to account for possible diel variability in biogeochemical properties. The objective of this high vertical

resolution sampling was to characterize changes in water chemistry and plankton community composition above, within, and below the DCM.

2.5. MESO-SCOPE Lagrangian Sampling

During the 2017 expedition, we extended our observations through Lagrangian sampling of the eddy centers using surface velocity program (SVP, Pacific Gyre) drifters with a drogue centered at 15 m depth. Initially, eddy centers were identified using shipboard ADCP measurements of upper ocean currents and underway hydrographic characterization conducted while transiting across the eddies. Using this information, a SVP drifter was deployed in the predicted center of each eddy (lowest current velocity and deepest or shallowest isopycnal depth). These drifters advanced in arcs consistent with the geostrophic flow. A second SVP drifter was then deployed near the center of the drift arcs to decrease the distance from the eddy center. The research vessel followed these secondary drifters conducting high-temporal resolution Lagrangian sampling over 3–4 days. The distance between the drifter and the ship at the Lagrangian sampling stations averaged 1.1 ± 0.8 (standard deviation) km, with a maximum distance of 4.1 km.

2.6. Biogeochemical Sample Collection and Analyses

The analytical methods used for assessing upper ocean biogeochemical properties, including concentrations of dissolved O_2 , chlorophyll, dissolved and particulate nutrients, and fluxes of particulate matter derived from sediment trap collections followed protocols utilized by the HOT program (<http://hahana.soest.hawaii.edu/hot/methods/results.html>). Briefly, concentrations of chlorophyll were determined from filtered seawater samples (25 mm diameter glass fiber filters; Whatman GF/F, nominal porosity 0.7 μm). Concentrations of chlorophyll *a* and phaeopigments were measured fluorometrically on a Turner Designs Model 10-AU fluorometer (Strickland & Parsons, 1972). Note that, in this environment, fluorescence from chlorophyll *b* is a major contributor to “phaeopigment” determinations (Karl, Bidigare, & Letelier, 2001). Seawater for subsequent determinations of particulate carbon (PC) and nitrogen (PN) was prefiltered through 202 μm Nitex® mesh screen, followed by positive pressure filtration onto precombusted 25 mm diameter glass fiber filters (Whatman GF/F). Filters were frozen at -20°C until analysis in the laboratory. Particulate carbon and PN concentrations were determined using an Exeter Analytical CE-440 CHN elemental analyzer (Exeter Analytical, UK) as described in Grabowski et al. (2019).

Samples for the determination of dissolved O_2 were collected into borosilicate flasks, fixed with manganous chloride and alkaline iodide, acidified, and dissolved O_2 concentrations were determined by titration with thiosulfate (Carpenter, 1965). Water samples for subsequent determinations of the sum of nitrate plus nitrite (hereafter $N + N$) and soluble reactive phosphorus (herein termed phosphate, PO_4^{3-}) concentrations were collected in acid-washed polyethylene bottles and stored frozen until analyzed using a SEAL Autoanalyzer III (Dore et al., 1996; Foreman et al., 2016). For most samples where $N + N$ concentrations were below 100 nM, concentrations were determined using a chemiluminescent method (Foreman et al., 2016). Iron (Fe) was sampled using a trace metal clean rosette and analyzed by inductively coupled plasma mass spectrometry after preconcentration by an automated SeaFAST system (Elemental Scientific; see Hawco et al. (2021), for full description).

2.7. Calculation of Isopycnal Anomalies and Nutrient Gradients

We calculated isopycnal concentration anomalies for inorganic nutrients and O_2 for both HL4 and MESO-SCOPE cruises to illustrate biogeochemical changes driven by past physical-biological processes in mesoscale eddies. These anomalies represent the concentrations of $N + N$, PO_4^{3-} , and O_2 measured along an isopycnal surface minus the cruise-averaged concentrations measured on the same isopycnal. Computing anomalies in this manner assumes similar initial concentrations of nutrients and O_2 for a given isopycnal surface, and that mesoscale physical-biological linkages drive variations in these properties.

Vertical gradients in inorganic nutrient concentrations were calculated as the slope of Model I linear regressions of nutrient concentration versus depth at depths between 10 m above the DCM and 90 m below the DCM from individual nutrient profiles collected during HL4 and MESO-SCOPE. We chose this portion of the water column because the vertical sampling resolution for nutrient concentrations was high enough to enable robust fitting of linear regressions; at shallower depths, $N + N$ concentrations are very low and generally do not demonstrate

vertical structure. The depth of the top of the nutricline was defined as the intercept on the depth axis of the linear regression used to compute $N + N$ vertical gradients, consistent with the approach adopted by Karl, Björkman, et al. (2001).

Isopycnal nutrient anomalies and vertical nutrient gradients were compared to near-monthly Eulerian observations conducted by the HOT program at Station ALOHA. These HOT program observations (1993–2020) were used to examine the relationships between SLA_{corr} and the O_2 and inorganic nutrient anomalies along the 24.5 kg m^{-3} isopycnal surface (henceforth, we refer to an isopycnal surface based on its potential density anomaly, which is the potential density - 1000 kg m^{-3}). For these analyses, we eliminated potential seasonal variability in O_2 and inorganic nutrient concentrations by subtracting the monthly mean isopycnal concentrations of these properties. For consistency, when comparing these anomalies with those observed during the HL4 and MESO-SCOPE cruises, we also subtracted the HOT monthly mean concentration from the isopycnal anomalies calculated on the eddy transects.

The calculation of vertical nutrient gradients on HOT observations followed the same procedure described for HL4 and MESO-SCOPE. Vertical profiles where less than three measurements existed in the vertical layer around the DCM were discarded for these analyses.

2.8. Plankton Abundance and Biomass

Abundances of picocyanobacteria (*Prochlorococcus* and *Synechococcus*) and pigmented eukaryotes (pico- and nanoplankton), together with non-pigmented picoplankton (hereafter, heterotrophic bacteria), were determined by flow cytometry. For these analyses, seawater was collected in 2 mL cryovials, fixed with microscopy-grade paraformaldehyde (0.24% vol/vol final concentration), stored in the dark for 15 min, flash frozen in liquid nitrogen, and stored at -80°C . Plankton were enumerated with an Influx (Cytospeia) flow cytometer, with pigmented cells distinguished based on their scattering and fluorescence characteristics using 2 excitation lasers (457 and 488 nm). The abundance of non-pigmented picoplankton (herein defined as heterotrophic bacteria) was determined by staining cells with SYBR Green I DNA and subtracting the contributions from *Prochlorococcus*.

The carbon biomass of larger (4–100 μm) eukaryotic phytoplankton was estimated by automated imaging flow cytometry (Imaging FlowCytobot [IFCB], McLane) over the course of the Lagrangian sampling in 2017. In both eddy centers, daily discrete samples were collected every 4 hr ($n = 6$ at each depth) at 15 m and at the DCM from Niskin[®] bottles mounted on the CTD rosette. Analyses were carried out within 2 hr of collection to ensure that cells were not deteriorating since samples were not preserved. The IFCB detects individual particles via laser-induced fluorescence and light scattering used to trigger image acquisition of all particles in successive $\sim 5 \text{ mL}$ samples.

A training set was used to classify the images to the genus level based on morphological traits, as described in Dugenne et al. (2020). The output of the random forest classifier (Sosik & Olson, 2007) was manually corrected to provide accurate estimates of cell size distribution and concentration for individual genera. For this study, we selected phytoplankton genera, then computed carbon biomass based on a biovolume-to-C quota using class-specific regression coefficients (Menden-Deuer & Lessard, 2000). Standard errors associated with the intercept and slope of the biovolume-to-C regressions result in a $\pm 20\%$ uncertainty in larger phytoplankton biomass.

2.9. Quantification of Particle Export

During the MESO-SCOPE cruise, 12 free-drifting, surface-tethered, sediment trap arrays were deployed along a line connecting the eddy centers (at approximately 18 km spacing) to examine the downward flux of sinking particulate material. Each surface-tethered array included 12 individual particle interceptor trap collector tubes (Knauer et al., 1979). Traps were deployed at 150 m for 10–13 days, collecting sinking particles. The sediment traps were prepared and processed following HOT program methods (Karl et al., 1996). Trap samples were processed and analyzed for PC, PN, particulate phosphorus (PPO_4^{3-}), PSi, particulate inorganic carbon (PIC; i.e., calcium carbonate), and stable nitrogen isotope composition in particles ($\delta^{15}\text{N-PN}$). In addition, sediment trap samples were used to quantify total mass of sinking particles. From the 12 individual collector tubes, 6 were processed for subsequent measurements of PC, PN, PIC, $\delta^{15}\text{N-PN}$; 3 were processed for PPO_4^{3-} ; and the remaining 3 traps were split and processed for PSi and total mass flux. Prior to filtration, trap contents were screened through

a 335- μm Nitex mesh to remove any mesozooplankton (swimmers) that are not part of the passive flux of particles. Collection tubes for subsequent analyses of PC, PN, and PIC were filtered onto 25 mm diameter combusted glass fiber filters, while samples for PPO_4^{3-} analyses were filtered onto combusted, acid-washed glass fiber filters. Samples for P_{Si} were filtered onto 47 mm diameter, 0.8 μm pore size polycarbonate filters. All filters were frozen until subsequent analyses. Filters for PC, PN, and $\delta^{15}\text{N}$ -PN were analyzed on a high-temperature elemental analyzer (Carlo Erba NC 2500) coupled to a Finnigan MAT DeltaS mass spectrometer. Filters for total mass were analyzed as described in Grabowski et al. (2019). Filters for PIC determinations were placed in gas-tight vials, fumed with phosphoric acid, and the CO_2 evolved in the headspace quantified by infrared absorption (Grabowski et al., 2019). Particulate silica analyses followed the NaOH digestion method for biogenic silica described in Brzezinski and Nelson (1989). Particulate organic carbon (POC) flux was calculated as the difference between PC and PIC.

3. Results

3.1. Transects Across Adjacent Eddies

The hydrographic and dynamic structure of the sampled eddies was consistent with expectations based on eddy polarity: cyclonic eddies were characterized by an uplifted thermocline and surface currents organized in a counterclockwise circulation, while anticyclones demonstrated deeper thermoclines and clockwise surface current circulation (Figure 1). In both cruises, surface currents were strongest along the frontal boundaries separating the adjacent eddies. During the HL4 cruise, frontal currents reached a maximum velocity of 0.85 m s^{-1} in the 11–61 m layer; during the MESO-SCOPE cruise in 2017, frontal currents reached a maximum velocity of 0.60 m s^{-1} . High horizontal resolution underway CTD profiles conducted during HL4 revealed the depth of the 19°C isotherm varied from 120 m in the cyclone center to 244 m in the anticyclone center (Figure 1d), while this isotherm varied between 79 m in the cyclone center to 255 m in the anticyclone center during MESO-SCOPE (Figure 1e). Similarly, the vertical position of isopycnal surfaces varied with eddy polarity. For example, during the HL4 cruise in 2016, the depth of the 25 kg m^{-3} isopycnal surface (typically occurring near the base of the DCM at Station ALOHA) deepened from 112 m near the cyclone center to 243 m near the anticyclone center (Figure 2), while this isopycnal varied from 84 m near the cyclone center to 220 m near the anticyclone center during the MESO-SCOPE cruise (Figure 2). This isopycnal was shallowest (80 m) in the northernmost station of the MESO-SCOPE cruise transect, reflecting the low SLA observed at this station, together with shallowing of isopycnals toward the northern edge of the NPSG.

Both of the cyclones and anticyclones sampled as part of this study represented extreme mesoscale events relative to historical Eulerian observations of SLA_{corr} at Station ALOHA (Figure 2). SLA_{corr} in the cyclone and anticyclone eddy centers averaged -18.4 and 23.8 cm during HL4 and -14.7 and 24.0 cm during MESO-SCOPE, respectively. In both cases, these SLA_{corr} values were more than two standard deviations different from the mean SLA_{corr} measured at Station ALOHA between 1993 and 2018 (Figures 2a and 2b).

The vertical position of the DCM also varied consistently with eddy polarity, with cyclones characterized by shallower DCM, but more intense chlorophyll fluorescence relative to anticyclones (Figures 2c and 2d). Moreover, during both cruises, but particularly during MESO-SCOPE, concentrations of dissolved O_2 in the cyclones peaked at depths shallower than the DCM, with O_2 concentrations greatest near the top of the 24.5 kg m^{-3} isopycnal in the cyclones, despite the DCM occurring closer to the 25 kg m^{-3} isopycnal (Figures 2e and 2f). Concentrations of O_2 along the 24.5 kg m^{-3} isopycnal were greatest in the cyclone sampled during the MESO-SCOPE cruise, peaking at $242.0 \text{ mmol m}^{-3}$ and decreasing to $220.9 \text{ mmol m}^{-3}$ in the center of the anticyclone (Figure 2). O_2 concentrations measured across the eddies as part of HL4 demonstrated similar patterns, with a peak concentration of $232.7 \text{ mmol m}^{-3}$ just below the 24.5 kg m^{-3} isopycnal in the cyclone and decreasing to a maximum $218.8 \text{ mmol m}^{-3}$ in the center of the anticyclone (Figure 2).

The observed eddy-dependent vertical changes in isopycnal surfaces resulted in displacement of inorganic nutrient concentrations, with upward displacement of $\text{N} + \text{N}$ concentrations below the DCM in cyclones, and downward displacement of isopycnals in anticyclones reducing concentrations of $\text{N} + \text{N}$ throughout the upper 200 m (Figures 2g and 2h). $\text{N} + \text{N}$ concentrations along the 24.5 kg m^{-3} isopycnal were elevated in the anticyclones (0.976 and $0.026 \text{ mmol m}^{-3}$ during HL4 and MESO-SCOPE, respectively), with lower concentrations in both cyclones ($<0.003 \text{ mmol m}^{-3}$; Figure 2). Along the 25 kg m^{-3} isopycnal, concentrations of $\text{N} + \text{N}$ ranged between

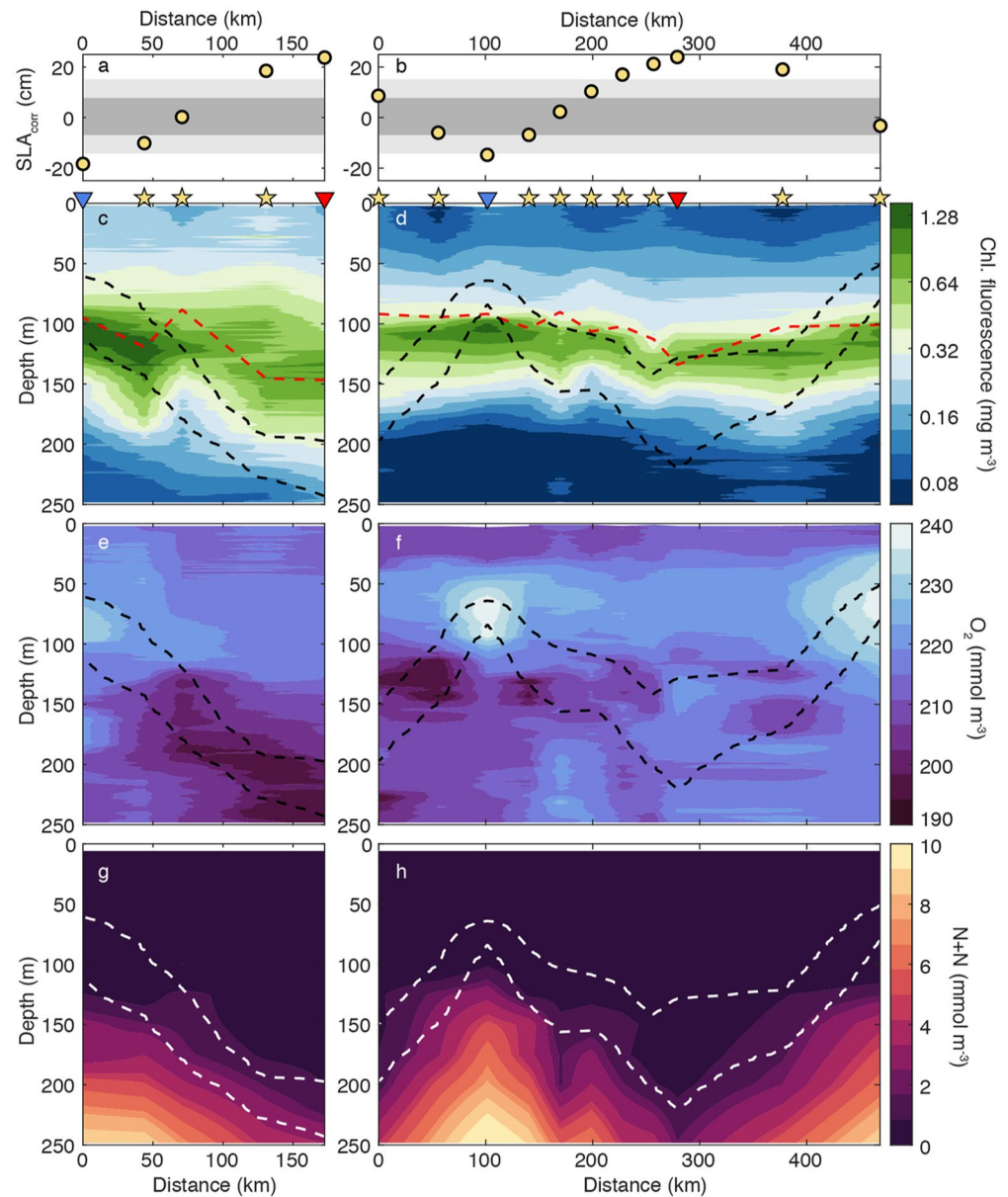


Figure 2. Biogeochemical characteristics along two transects between the couple of adjacent eddies sampled during HL4 in 2016 (panels a, c, e, and g) and MESO-SCOPE in 2017 (panels b, d, f, and h). (a and b) SLA_{corr} at stations sampled during transects across adjacent eddies (black symbols). Shaded areas represent variability in SLA_{corr} at Station ALOHA between 1993 and 2018, with dark gray shading depicting ± 1 standard deviation of the mean and light gray shading depicting ± 2 standard deviations from the time-averaged SLA_{corr} value; (c and d) chlorophyll (Chl) fluorescence, (e and f) dissolved O_2 concentrations, and (g and h) concentrations of $N + N$ during adjacent eddy sampling transects. Black or white dashed lines depict the depth of isopycnal surfaces with potential density anomaly of 24.5 kg m^{-3} (shallower surface), and 25 kg m^{-3} (deeper surface). Red dashed lines in panels c and d depict the depth of the top of the nutricline. Symbols on the top panels depict the position of the sampling stations along the transects, with blue and red triangles depicting the stations closest to the cyclone and the anticyclone centers, respectively.

0.002 and $2.975 \text{ mmol N m}^{-3}$ during MESO-SCOPE, and between 3.584 and $0.875 \text{ mmol N m}^{-3}$ during HL4, across all stations.

For both cruises, daily integrated incident PAR reaching both the DCMs and the 24.5 kg m^{-3} isopycnal surface was significantly greater in cyclones than in anticyclones (Wilcoxon rank sum test, $p = 0.03$; Table 1). However,

Table 1

Daily-Integrated Downwelling PAR Irradiance ($\text{mol Photon m}^{-2} \text{d}^{-1}$) Measured in the Eddy Centers at Three Vertical Levels: (a) Above the Sea Surface, (b) at the Depth of the Deep Chlorophyll Maximum (DCM), and (c) at the Depth of the 24.5 kg m^{-3} Isopycnal Surface

	HOE-Legacy 4		MESO-SCOPE					
	Cyclone	Anticyclone	Cyclone			Anticyclone		
Day	May 11	May 12	Jul 4	Jul 5	Jul 6	Jul 9	Jul 10	Jul 11
Surface PAR	50	40.2	40.5	53.4	51.9	50.6	51.9	48.5
DCM depth	103 ± 4	145 ± 8	104 ± 6	104 ± 4	107 ± 4	121 ± 7	125 ± 5	123 ± 2
DCM PAR	0.56	0.14	0.26	0.49	0.51	0.23	0.21	0.21
24.5 isopyc. depth	61 ± 6	197 ± 7	69 ± 5	70 ± 4	68 ± 6	128 ± 6	130 ± 7	128 ± 3
24.5 isopyc. PAR	3.42	0.016	1.6	3.05	3.37	0.15	0.17	0.17

Note. The depths of the DCM and of the isopycnal surface (m) are daily averages \pm standard deviations from shipboard conductivity, temperature, and depth measurements.

differences in downwelling irradiance at the depth of the DCM were not significantly different between the two eddies sampled during the MESO-SCOPE cruise (Wilcoxon rank sum test $p = 0.05$).

3.2. Isopycnal Anomalies of O_2 and Inorganic Nutrients

Depth-dependent oscillations in the thermocline appear to underlie much of the variability associated with concentrations of inorganic nutrients and dissolved O_2 (Figures 2g and 2h). However, analyses of these properties along isopycnal surfaces revealed more subtle dynamics. For both cruises, robust anomalies for both O_2 and inorganic nutrients were observed along isopycnal surfaces located at depths surrounding the DCM. The isopycnal anomalies in cyclonic eddies were consistently positive for O_2 (Figures 3a and 3b) and consistently negative for $\text{N} + \text{N}$ and PO_4^{3-} (Figures 3c–3f), indicative of prior net phytoplankton production. Anomalies associated with anticyclones demonstrated less robust mesoscale variation: for example, during the HL4 anticyclone anomalies associated with $\text{N} + \text{N}$, PO_4^{3-} , and O_2 near the DCM had the opposite sign of those measured in the cyclone, while during MESO-SCOPE inorganic nutrient anomalies near the DCM had the same sign in both the cyclone and anticyclone (Figure 3).

To assess the generality of mesoscale variability in biogeochemistry along isopycnal surfaces located near the depth of the DCM, we evaluated relationships between SLA_{corr} and both O_2 and inorganic nutrient anomalies along the 24.5 kg m^{-3} surface using historical HOT program measurements (Figure 4). These analyses revealed consistent patterns in both the HOT program observations and the eddy transects. In particular, the seasonally detrended O_2 concentration anomalies decreased with increasing SLA_{corr} , while the de-seasoned concentration anomalies of both $\text{N} + \text{N}$ and PO_4^{3-} increased with SLA_{corr} (Figure 4). The consistency in concentrations of O_2 and inorganic nutrients to variations in SLA_{corr} along this isopycnal surface suggests the patterns we observed are not specific to strong mesoscale eddies, but rather are more generally reflective of the full range of mesoscale motions observed in the region near Station ALOHA. Slopes of the isopycnal concentration anomalies versus SLA_{corr} (Model II geometric mean regression) were $-1.07 \pm 0.07 \text{ mmol O}_2 \text{ m}^{-3} \text{ cm}^{-1}$, $0.102 \pm 0.008 \text{ mmol N} + \text{N m}^{-3} \text{ cm}^{-1}$ and $0.00860 \pm 0.00067 \text{ mmol PO}_4^{3-} \text{ m}^{-3} \text{ cm}^{-1}$. The resulting ratios of these slopes were -10.49 (mol O_2 : mol N), -124.4 (mol O_2 : mol P), and 11.86 (mol N : mol P). SLA_{corr} explained less of the variability in the inorganic nutrient concentration anomalies than O_2 concentration anomalies (correlation coefficients values for O_2 , $\text{N} + \text{N}$, and PO_4^{3-} were -0.49 , 0.21 , and 0.23 , respectively, all with $p < 0.001$), and departure from a linear relationship are particularly evident for $\text{N} + \text{N}$ at low values of SLA_{corr} (i.e., when SLA_{corr} decreases below -10 cm , such as would occur with relatively strong cyclonic eddies). Potential Fe limitation of DCM plankton production was also investigated during the MESO-SCOPE cruise and results from that study are described elsewhere (Hawco et al., 2021). Briefly, dissolved Fe was depleted in the lower euphotic zone of the cyclone, averaging 73 nmol m^{-3} at a potential density of $\sim 25.16 \text{ kg m}^{-3}$, the same isopycnal where we measured the maximum cyclonic deficit of $\text{N} + \text{N}$ and PO_4^{3-} . In this layer, the cyclone had 110 nmol m^{-3} less Fe than the anticyclone as

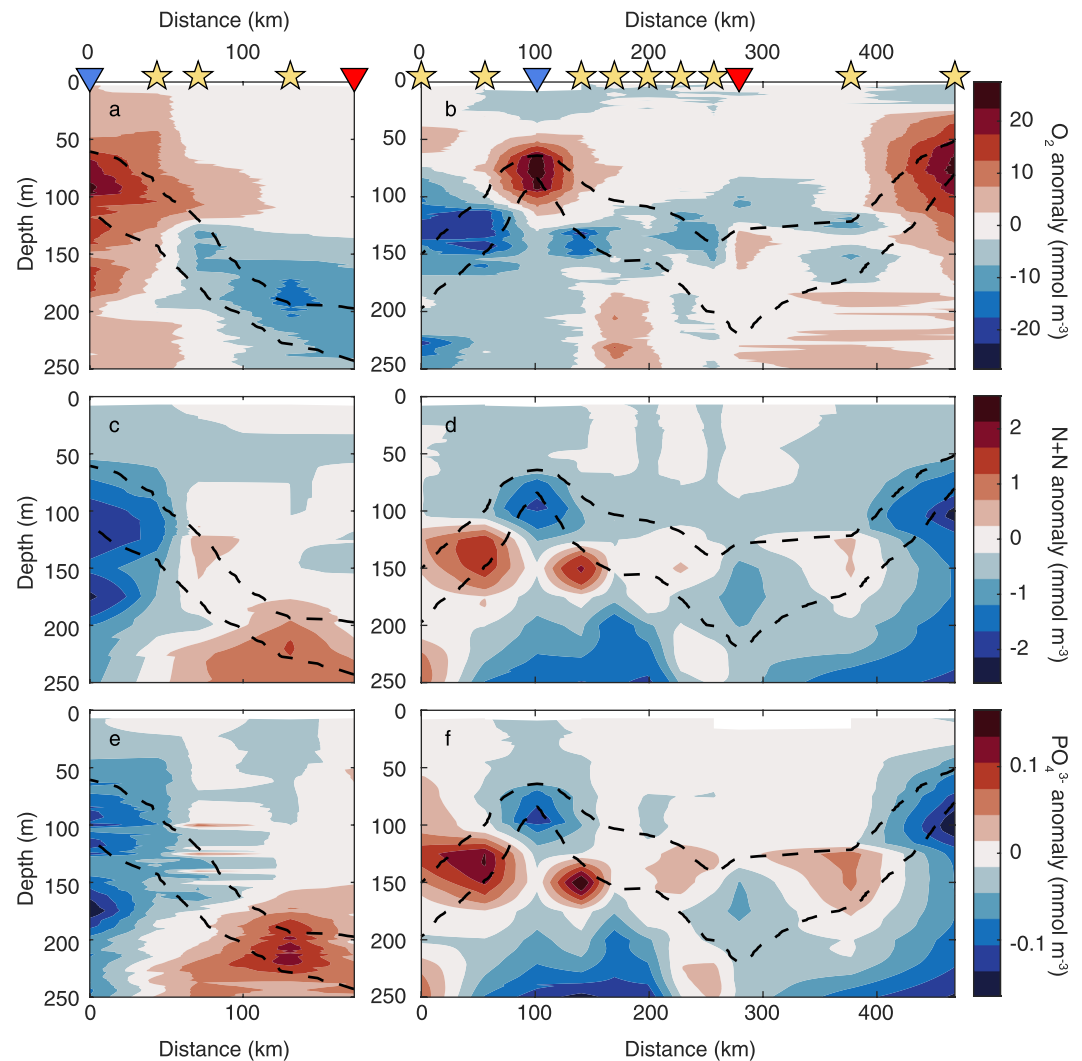


Figure 3. Concentration anomalies of (a and b) O_2 , (c and d) $N + N$, and (e and f) PO_4^{3-} with respect to the mean isopycnal concentration measured during sampling transects of adjacent eddies during (a, c, and e) HL4 and (b, d, and f) MESO-SCOPE. Dashed lines depict the depth of potential density anomaly isopycnal surfaces of 24.5 kg m^{-3} (shallower surface), and 25 kg m^{-3} (deeper surface). Symbols on the top panels depict the position of the sampling stations along the transect, with blue and red triangles depicting the stations closest to the cyclone and the anticyclone centers, respectively.

compared with 1.80 mmol m^{-3} and 0.11 mmol m^{-3} decreases in $N + N$ and PO_4^{3-} , respectively. Lower dissolved Fe at 25.16 kg m^{-3} in the cyclonic eddy is consistent with biological Fe uptake by phytoplankton.

The isopycnal anomalies of O_2 and inorganic nutrients vary inversely due to primary production and mineralization, which produce O_2 and consume inorganic nutrients (or vice versa) in proportions that are relatively invariant across ocean basin scales (Anderson & Sarmiento, 1994; Redfield, 1958). To assess if the isopycnal variations of O_2 and inorganic nutrients in mesoscale eddies were consistent with the stoichiometry of the production and consumption of organic matter, we calculated the excess O_2 anomaly as follows:

$$\text{isopycnal anomaly of } (O_2 - O_2 \text{ solubility}) + 10.5 \times \text{isopycnal anomaly of } (NO_3^- + NO_2^-)$$

where 10.5 represents the moles of O_2 produced when 1 mol of $NO_3^- + NO_2^-$ is consumed for the synthesis of new organic matter, or the inverse for its consumption (Anderson, 1995; Johnson et al., 2010). For this analysis, we also subtracted O_2 solubility to avoid misinterpreting variations caused by changes in hydrography along the eddy transects. The excess O_2 anomaly was positive in both cyclone centers in a vertical layer located just above the DCM and approximately between 50 and 100 m (Figure 5a). In this layer, the excess O_2 anomaly reached

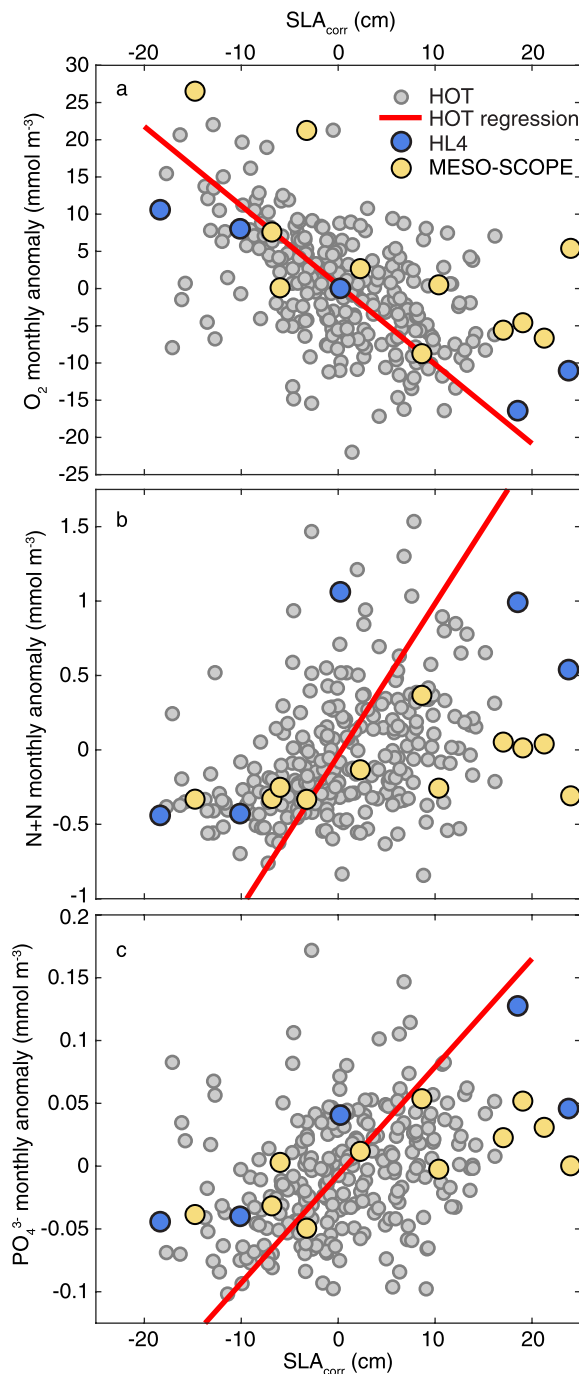


Figure 4. Monthly isopycnal anomalies of the concentrations of (a) O_2 , (b) $N + N$, and (c) PO_4^{3-} versus SLA_{corr} from Hawaii Ocean Time-series (HOT) program measurements (gray symbols), the HL4 eddy transect (blue symbols), and the MESO-SCOPE eddy transect (yellow symbols) along the 24.5 kg m^{-3} density surface. Red lines depict the Model II geometric mean regression of HOT observations. Note that for visual clarity the y-axes exclude 3 observations with high concentration anomalies of $N + N$ (2.4, 4.4, and 8.2 mmol m^{-3} corresponding to SLA_{corr} of 8.4, -4.7 , and 1.4 cm , respectively) and 2 observations with high concentration anomalies of PO_4^{3-} (0.28 and 0.56 mmol m^{-3} corresponding to SLA_{corr} of -4.7 , and 1.4 cm , respectively).

values above 10 mmol m^{-3} in cyclones, while it was close to 0 or negative in both anticyclones (Figure 5). The excess O_2 anomaly was predominantly negative below 100 m in all four eddy centers (Figure 5), indicating that the O_2 concentration in these eddy centers was lower than expected assuming the water started with the average isopycnal concentrations measured along the transect and was later modified assuming fixed $10.5 O_2:N$ (mol:mol) stoichiometry (Anderson, 1995).

3.3. Vertical Gradients and Mixing Estimates at the Top of the Nutricline

We calculated how mesoscale motions influenced vertical gradients in $N + N$ and PO_4^{3-} based on the slopes of nutrient concentration versus depth relationships calculated from the individual nutrient profiles. Upward displacement of the nutricline associated with cyclonic eddies resulted in vertical gradients in $N + N$ that were 1.8–9.2 times greater near the center of the cyclones than in the anticyclones (Figures 6a and 6b). Similarly, vertical gradients in PO_4^{3-} were 1.8–10.8 times greater near the center of the cyclones than in the anticyclones (Figures 6c and 6d). Changes in the gradients of $N + N$ and PO_4^{3-} between cyclones and anticyclones were even larger when derived based on nutrient concentrations measured from high-resolution vertical sampling at depths around the DCM.

We also examined relationships between the vertical nutrient gradients and SLA_{corr} based on the historical HOT program observations (Figures 6e and 6f). These analyses revealed patterns consistent with the more limited observations during HL4 and MESO-SCOPE. Specifically, vertical gradients in concentrations of $N + N$ and PO_4^{3-} decreased with increases in SLA_{corr} (Figures 6e and 6f).

3.4. Mesoscale Variability in Plankton Biomass and Community Composition

Several consistent patterns in the near-surface waters and at the DCM emerged based on various proxy measurements of plankton biomass at the centers of both pairs of cyclones and anticyclones. In the near-surface waters, there were no apparent eddy-specific differences in concentrations of PC or beam attenuation, nor in chlorophyll *a* concentrations or fluorescence (Figure 7). In contrast, at the depth of the DCM, all of these proxy measurements of plankton biomass were elevated in the cyclonic eddies relative to the anticyclones. The concentration of PC was greater in the DCM of the cyclones relative to anticyclones by 1.3- and 1.4-fold, in the two expeditions (Figure 7a). Similarly, the concentration of chlorophyll *a* was greater in the DCM of the cyclones relative to anticyclones by 1.2- and 1.3-fold (Figure 7c). This difference was even more pronounced for in situ chlorophyll fluorescence (Figure 7d), which includes contributions from pigments other than chlorophyll *a* and can be influenced by variation in fluorescence yield (Roesler et al., 2017). Fluorescence in the DCM was 1.3- and 1.8-fold greater in the cyclonic eddies than in the anticyclones (Figure 7d). Similarly, beam attenuation, an optical proxy for particle concentrations, was 1.4- and 1.5-fold greater at the depth of DCM in the cyclonic eddies relative to the anticyclones (Figure 7b) suggesting enhancement of plankton biomass rather than photoacclimation as drivers of these signals.

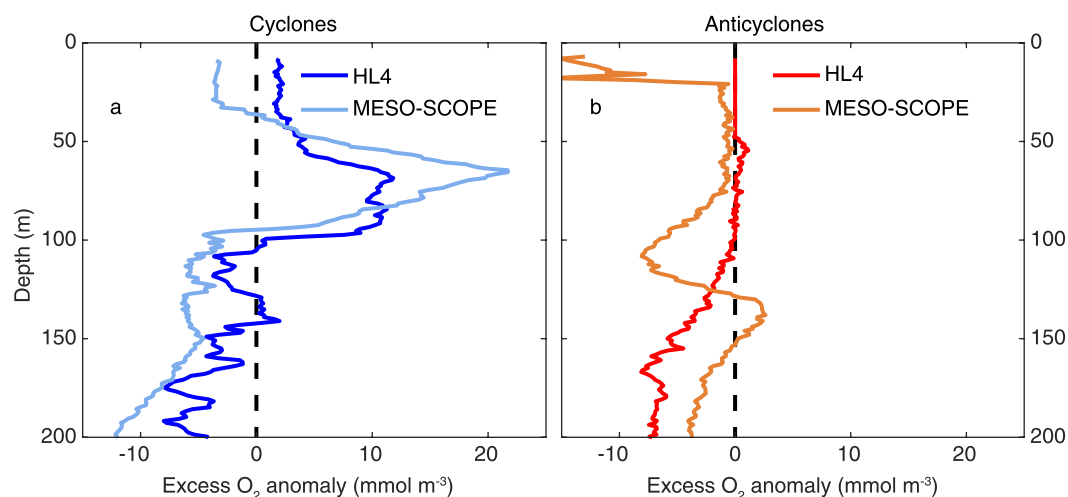


Figure 5. Excess O_2 anomaly in (a) cyclones and (b) anticyclones. Excess O_2 anomaly reflects the surplus of O_2 with respect to the concentration expected if starting from the average isopycnal concentrations of O_2 and $N + N$ along the transects and assuming that they are modified following a fixed $-10.5 O_2:N$ (mol:mol) stoichiometry.

We also evaluated the abundances of *Prochlorococcus*, *Synechococcus*, eukaryotic phytoplankton, and heterotrophic bacteria in the adjacent eddy pairs based on flow cytometric analyses. We found that *Prochlorococcus* abundances were greater in the waters above the DCM in both anticyclones, relative to the cyclones, and relative to the HOT program climatology (Figures 8a and 8e). In contrast, eukaryotic phytoplankton (restricted to pico- and nanoplankton) abundance was elevated in a broad layer near the DCM. Maximum abundance in this layer exceeded the 95th percentile of HOT observations, with abundances in these eddies $>4,000$ cells mL^{-1} (Figures 8c and 8g). Eukaryotic phytoplankton abundances in the near-surface waters were similar among the sampled eddies. Vertical distributions of *Synechococcus* were similar among the sampled eddies and similar to the HOT program observations of this genus (Figures 8b and 8f). Heterotrophic bacteria were more abundant in anticyclones than in cyclones in the near-surface and in waters below the DCM, but this pattern was reversed at depths just above the DCM.

During the MESO-SCOPE cruise, we also examined eddy-driven variability in the biomass of larger eukaryotic phytoplankton cells (4–100 μm in equivalent spherical diameter) imaged with an IFCB. In the near-surface waters, biomass estimates of most of the enumerated phytoplankton were similar between the eddies, with the exception of significantly greater biomass of Prymnesiophyceae in the anticyclone (Figure 9, Wilcoxon rank sum test, $p < 0.05$). Conversely, at the depth of the DCM, most phytoplankton classes demonstrated greater biomass in the cyclone than in the anticyclone (Figure 9). The dominant classes in the DCM of the cyclone were Prymnesiophyceae and Bacillariophyceae (specifically members of diatoms), whose biomass was 2.3 and 4.7 times greater than in the anticyclone, respectively (Figure 9b). Prymnesiophyceae genera, whose biomass was significantly larger in the DCM of the cyclone compared to the anticyclone (Wilcoxon rank sum test, $p < 0.05$), included *Phaeocystis*, *Ophiaster*, *Umbellosphaera*, *Acanthoica*, *Gephyrocapsa*, and *Syracosphaera* (in descending order of average biomass). The Bacillariophyceae genera enriched in the DCM of the cyclone were *Pseudo-nitzschia*, *Chaetoceros*, *Cylindrotheca*, and *Navicula*. Members of the Prymnesiophyceae and Bacillariophyceae are important controls on the formation of calcium carbonate and opal, respectively.

3.5. Mesoscale Variability in Particle Export

Drift tracks of the sediment trap arrays were consistent with geostrophic circulation of the two eddies sampled during MESO-SCOPE (Figures 10a and 10b). The resulting particle fluxes measured across the adjacent eddies revealed clear mesoscale structure in both the magnitude and stoichiometry of exported particulate matter. Most notably, despite similarities in POC, PN, and PPO_4^{3-} fluxes across the eddies, total mass, P_{Si}, and PIC export were approximately 2–, 4–, and 2.9–fold greater, respectively, in the cyclone relative to the anticyclone (Figures 10c and 10d; Supporting Information Table S1). Moreover, total mass, P_{Si}, and PIC fluxes were all inversely related to SLA_{corr} (Figures 10c and 10d; Supporting Information Table S1). In contrast, fluxes of POC, PN, and

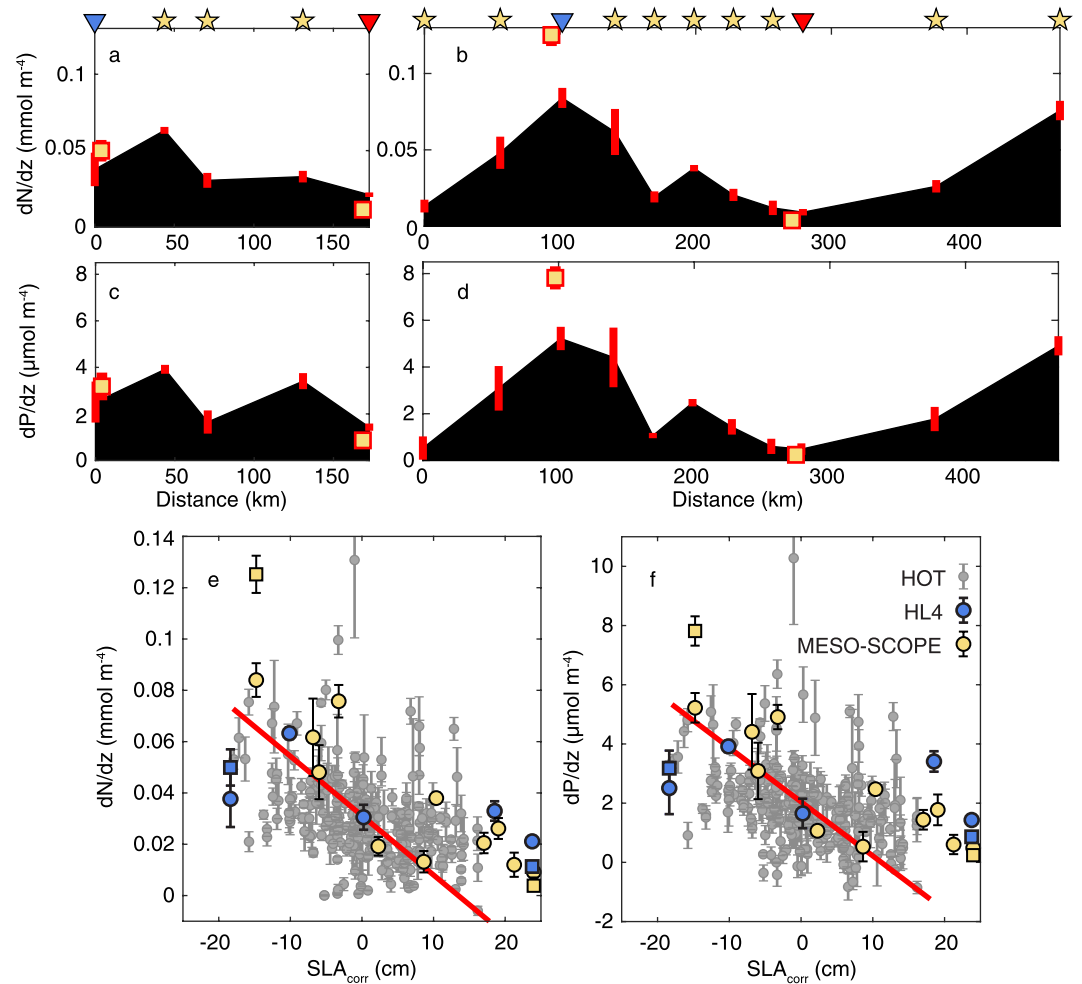


Figure 6. Changes in the vertical gradients of (a and b) N + N and (c and d) PO_4^{3-} , defined as dN/dz and dP/dz , respectively, across adjacent eddies of opposite polarity for (a and c) HLA and (b and d) MESO-SCOPE cruises. Panels e and f depict vertical gradients in N + N and PO_4^{3-} concentrations, respectively, versus SLA_{corr} for the two eddy transects (blue and yellow symbols) and the Hawaii Ocean Time-series (HOT) program observations (gray symbols). Yellow squares in (a–d) and blue or yellow squares in (e–f) depict gradients estimated from the high vertical resolution profiles in the four eddy centers. Red lines in (a–d) and error bars in (e–f) depict ± 1 standard deviation in the slopes. Red lines in (e–f) are linear regressions on HOT program nutrient gradients (Model II) with slopes of -0.0023 ± 0.0002 mmol m^{-4} cm^{-1} ($r = 0.36$, $p = 5 \times 10^{-9}$) and -0.00018 ± 0.00001 mmol m^{-4} cm^{-1} ($r = 0.35$, $p = 1 \times 10^{-8}$) for N + N and PO_4^{3-} , respectively. Estimates of vertical nutrient gradients were obtained by calculating the slope of the Model I linear regression of nutrient concentration versus depth in the vertical layer between 10 m above and 90 m below the depth of the deep chlorophyll maximum.

PP_4^{3-} did not vary significantly with spatial variations in SLA_{corr} (Figure 10; Supporting Information Table S1; Model II least-squares linear regressions, $p > 0.05$). In the cyclone, export of PIC accounted for 17% of the PC flux, with PIC comprising a lower fraction ($\sim 10\%$) of PC flux in the anticyclone (Table 2). The proportions of PIC and PSi to mass flux were inversely related to spatial changes in SLA_{corr} , with PIC:mass flux ratios (g $CaCO_3$:g mass) decreasing from 38% to 28%, and PSi: Mass flux ratios (g SiO_2 : g mass) varying from 5.8% to 2.1% across the cyclone to anticyclone transect (Table 2). Because of the proportionally greater contribution of PIC and PSi to mass flux in the cyclonic eddy, POC to mass flux (g C: g mass) was positively related to SLA_{corr} , with POC representing upwards of 34% of mass flux in the anticyclone and only $\sim 22\%$ in the cyclone (Table 2). In addition to evaluating mesoscale spatial variation in fluxes of key bioelements, we also quantified changes in $\delta^{15}N$ -PN. The $\delta^{15}N$ -PN of exported particles was inversely related to changes in SLA_{corr} across the dipole, with the cyclone exporting PN with a $\delta^{15}N$ signature as great as $\sim 4.3\text{‰}$, decreasing to as low as 3.0‰ in the anticyclone (Table 2).

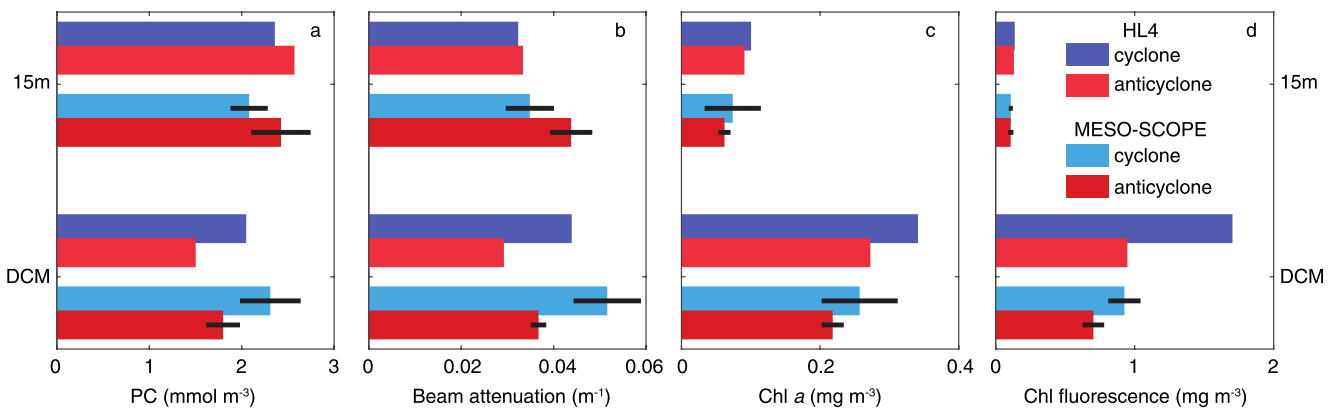


Figure 7. Average particle and pigment concentrations at 15 m and at the depth of the deep chlorophyll maximum (DCM) in the centers of the cyclones (blue) and anticyclones (red) sampled as part of this study. Panels (a) and (b) depict the concentrations of particulate carbon (PC) and in situ optical measurements of beam attenuation, respectively. Panels (c) and (d) depict the concentration of chlorophyll *a* (Chl *a*) and in situ optical measurements of chlorophyll fluorescence, respectively. Data points in panels (b) and (d) were isolated from the same deployments and depths used in samples (a) and (c). Black lines depict ± 1 standard deviation of the mean, and are absent when only 1 measurement was available. The top 4 bars depict observations from 15 m, while the bottom 4 bars depict observations from the DCM. For the HOE-Legacy 4 cruise, the concentrations of PC and chlorophyll *a* at 15 m were obtained by averaging measurements collected at 5 and 25 m. For the MESO-SCOPE cruise, measurements associated with the Lagrangian sampling periods were used.

The elevated contributions of PSi and PIC to particle export in the cyclonic eddy resulted in significant spatial differences in the elemental stoichiometry of particulate matter export across the mesoscale field. Elevated PSi flux in the cyclone coincided with decreasing POC:PSi, PN:PSi, and PPO_4^{3-} :PSi ratios (mol:mol) across the eddies (Table 2). Moreover, all three ratios were positively correlated to changes in SLA_{corr} . Elevated fluxes of PIC within the cyclonic eddy resulted in decreasing PC:PIC, PN:PIC, and PPO_4^{3-} :PIC ratios across the cyclone to anticyclone transect, with all three ratios inversely related to spatial changes in SLA_{corr} (Table 2). In contrast,

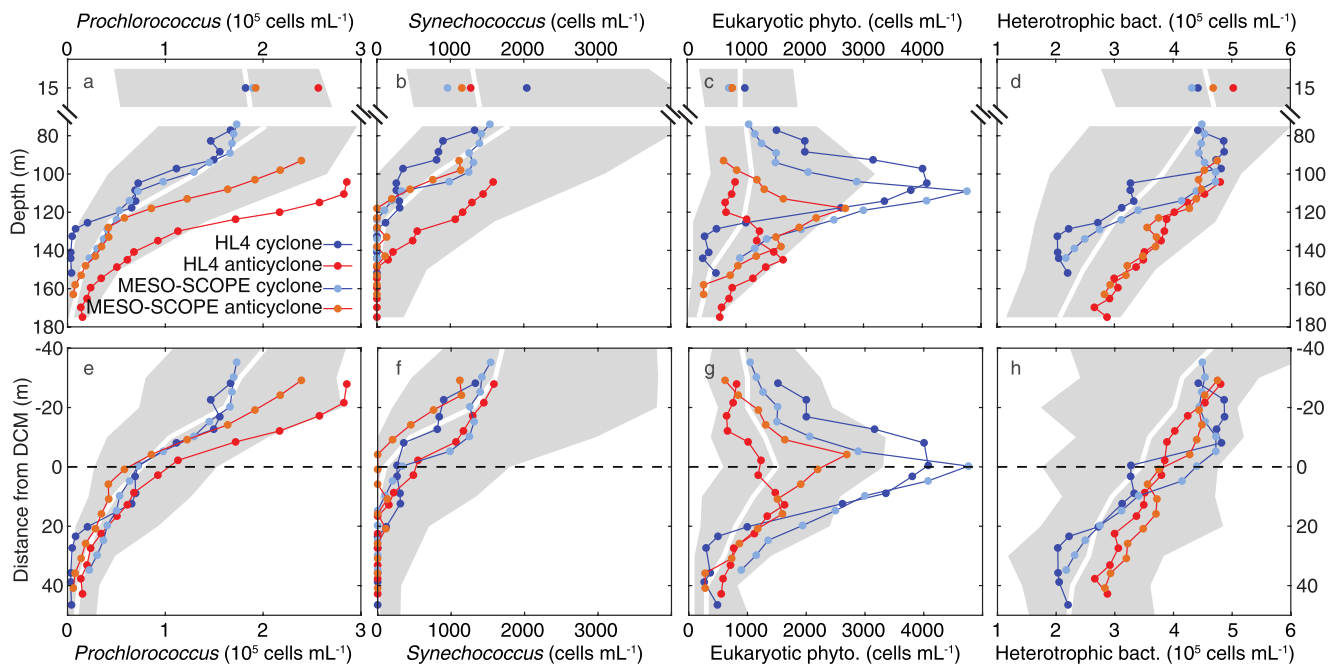


Figure 8. Average abundances of *Prochlorococcus*, *Synechococcus*, eukaryotic phytoplankton, and heterotrophic bacteria in the centers of the adjacent eddies derived from flow cytometry. Panels (a–d) depict vertical profiles of cell abundances at depths bracketing the deep chlorophyll maximum (DCM) in each eddy; the mean cell abundances measured at 15 m are also shown. Panels (e–h) depict the same profiles shown in panels (a–d), but the vertical axes are scaled relative to the depth of the DCM (positive values are deeper). White lines depict the median and shaded areas are the 5th and 95th percentiles of HOT program measurements of these abundances. For the HOE-Legacy 4 cruise, abundances at 15 m were calculated as the average of measurements at 5 and 25 m. For the MESO-SCOPE cruise, abundances are averaged from sample collections during the Lagrangian sampling periods.

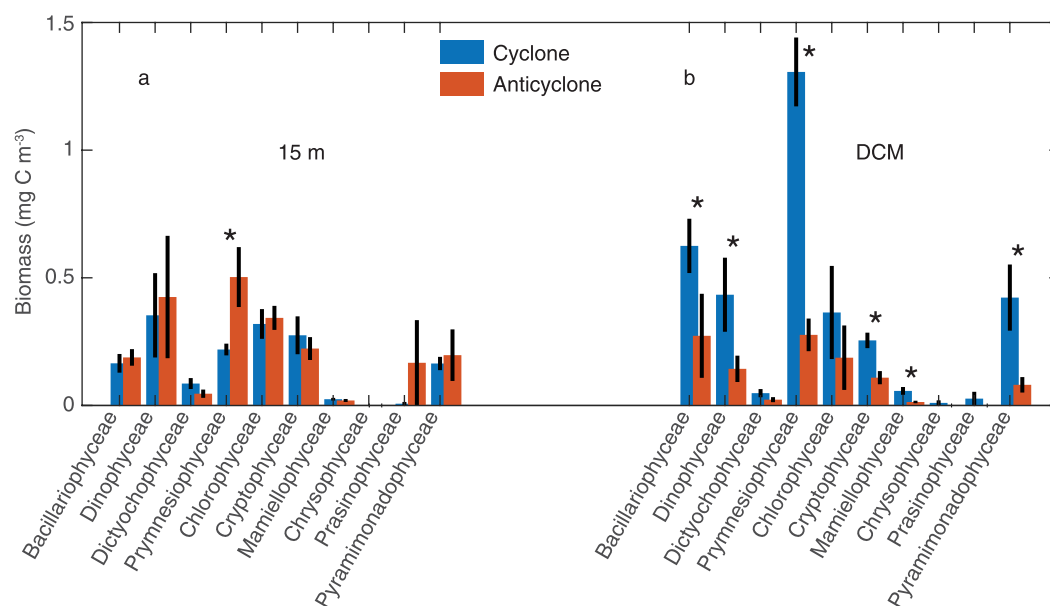


Figure 9. Mean biomass of nano- and microplanktonic (4–100 μm diameter) phytoplankton cells in the (a) near-surface ocean and (b) at the depth of the deep chlorophyll maximum at the cyclone (blue bars) and anticyclone (red bars) centers sampled during the MESO-SCOPE cruise. Bars depict mean of 7–8 discrete samples collected over 1 day and error bars are ± 1 standard error of the mean. Asterisks depict significant differences in biomass between cyclones and anticyclones (Wilcoxon rank sum test, $p < 0.05$).

POC:PPO₄³⁻ and PN:PPO₄³⁻ ratios (mol:mol) did not vary with SLA_{corr}, averaging 173 (± 20) and 28 (± 2.0), respectively. Intriguingly, although neither POC nor PN fluxes varied significantly with SLA_{corr}, the ratio of POC:PN was inversely and significantly related to SLA_{corr} (Table 2).

Once again, we leveraged HOT program observations to evaluate the generality of the mesoscale variability of particle fluxes across eddies. In this instance, we assessed the significance and strength of the Pearson correlations between HOT particle fluxes and SLA_{corr}. Consistent with our sampling during MESO-SCOPE, we find a lack of correlation between SLA_{corr} and sinking fluxes of PC, PN, and PPO₄³⁻, but significant negative correlations in fluxes of both P_{Si} and P_{IC} and SLA_{corr} (in the Supporting Information Table S1; $p < 0.05$). While the negative correlations of P_{Si} and P_{IC} are consistent with observations during MESO-SCOPE, we also found a significant positive correlation for HOT observations between $\delta^{15}\text{N}$ and SLA_{corr} (correlation coefficient of 0.14; $p < 0.05$), which was opposite in sign of the relationship observed based on the MESO-SCOPE sediment trap collections.

4. Discussion

4.1. Mesoscale Impacts on the Nutricline and Lower Euphotic Zone

On two separate research cruises in the subtropical North Pacific Ocean, we sampled pairs of adjacent mesoscale eddies of opposite polarity in late spring and summer, providing an opportunity for comparative analyses of upper ocean biogeochemistry and plankton ecology associated with mesoscale features in close spatial proximity (<200 km). By coupling our sampling of adjacent eddies with a multi-decadal analysis of HOT program observations, we find robust differences between cyclones and anticyclones in concentrations of chlorophyll *a*, dissolved O₂, inorganic nutrients, and particle load in the lower euphotic zone. However, differences in these properties were not apparent in the well-lit upper ocean waters.

The consistent biogeochemical responses to mesoscale motions observed in the lower euphotic zone reflect rapid plankton assimilation of nutrients as the nutricline undergoes mesoscale-driven oscillations across the exponentially varying light field. This variability in the lower euphotic zone is consistent with previous findings on the change in the vertical distributions of nutrients and biomass related to mesoscale activity at Station ALOHA (Barone et al., 2019; Church et al., 2009). The eddies sampled as part of this study bracketed the full dynamic

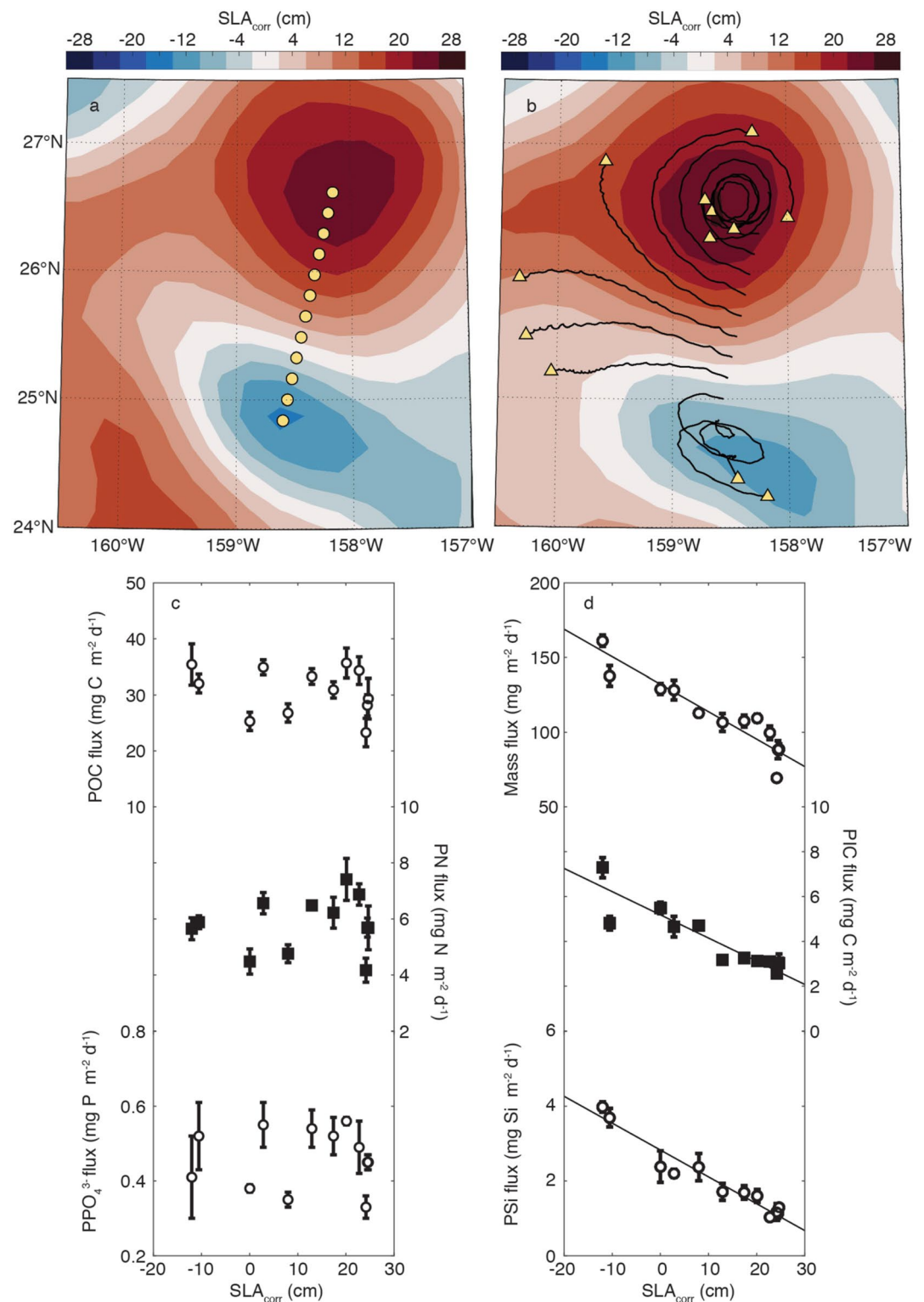


Figure 10. Results from sediment trap array deployments during the MESO-SCOPE eddy survey. (a) Coordinates of the 12 individual, free-drifting particle interceptor trap arrays at the time of deployment superimposed on the map of SLA_{corr} for July 2; (b) spatial drift tracks of the particle interceptor traps deployed during the MESO-SCOPE expedition superimposed on the map of SLA_{corr} on July 14, where yellow triangles depict locations of sediment trap recovery at the end of the collection period; (c) variability of the fluxes of particulate organic carbon, particulate nitrogen, and PPO_4^{3-} with SLA_{corr}; (d) relationships between fluxes of total mass, particulate inorganic carbon, and particulate silica with SLA_{corr}. Lines in (d) depict the Model II linear regressions.

Table 2
Stoichiometry and $\delta^{15}\text{N}$ Signature of Particulate Matter Exported During the MESO-SCOPE Cruise

Station	SLA (cm)	POC:Mass (g C:g)	PIC:Mass (g CaCO_3 :g)	PSi:Mass* (g SiO_2 :g)	PIC:PC (mol:mol)	POC:PN (mol:mol)	POC:PSi (mol:mol)	PN:PSi (mol:mol)	PN:PIC (mol:mol)	$\delta^{15}\text{N}$ -PN
1	-12.0	0.22 ± 0.02	0.38 ± 0.02	0.053 ± 0.002	0.17 ± 0.02	7.3 ± 0.9	21 ± 2	2.8 ± 0.2	0.66 ± 0.06	4.3 ± 0.21
2	-10.5	0.23 ± 0.02	0.29 ± 0.02	0.058 ± 0.005	0.13 ± 0.01	6.4 ± 0.4	20 ± 2	3.2 ± 0.2	1.05 ± 0.08	4.3 ± 0.10
3	0.0	0.20 ± 0.01	0.36 ± 0.02	0.039 ± 0.007	0.18 ± 0.01	6.6 ± 0.8	25 ± 5	3.8 ± 0.8	0.70 ± 0.08	3.8 ± 0.25
4	2.8	0.27 ± 0.02	0.30 ± 0.03	0.036 ± 0.003	0.12 ± 0.01	6.2 ± 0.4	37 ± 2	6.0 ± 0.5	1.21 ± 0.14	3.8 ± 0.10
5	8.0	0.24 ± 0.02	0.35 ± 0.01	0.045 ± 0.007	0.15 ± 0.01	6.6 ± 0.6	26 ± 4	4.0 ± 0.7	0.87 ± 0.06	4.2 ± 0.40
6	12.9	0.31 ± 0.02	0.25 ± 0.02	0.034 ± 0.005	0.09 ± 0.01	6.0 ± 0.3	46 ± 6	7.6 ± 1.0	1.75 ± 0.10	4.0 ± 0.07
7	17.4	0.29 ± 0.02	0.25 ± 0.01	0.034 ± 0.004	0.10 ± 0.00	5.8 ± 0.6	43 ± 5	7.4 ± 1.0	1.64 ± 0.15	3.8 ± 0.12
8	20.1	0.33 ± 0.03	0.23 ± 0.01	0.032 ± 0.004	0.08 ± 0.01	5.6 ± 0.7	52 ± 7	9.3 ± 1.4	2.04 ± 0.22	3.8 ± 0.15
9	22.8	0.34 ± 0.03	0.26 ± 0.02	0.021 ± 0.002	0.08 ± 0.01	5.8 ± 0.5	78 ± 8	13 ± 1.2	1.90 ± 0.12	3.6 ± 0.07
10	24.2	0.34 ± 0.04	0.31 ± 0.01	0.036 ± 0.007	0.10 ± 0.01	6.5 ± 1.0	47 ± 10	7.2 ± 1.5	1.40 ± 0.15	3.4 ± 0.15
11	24.7	0.33 ± 0.04	0.28 ± 0.04	0.032 ± 0.002	0.09 ± 0.02	6.0 ± 1.1	53 ± 7	8.8 ± 1.3	1.61 ± 0.31	3.0 ± 0.00
12	24.5	0.32 ± 0.03	0.28 ± 0.02	0.028 ± 0.003	0.10 ± 0.01	5.8 ± 0.5	58 ± 8	10.0 ± 1.3	1.60 ± 0.11	3.5 ± 0.06
Slope (units cm^{-1})		0.0038 ± 0.0005	-3.4 · 10 ⁻³ ± 0.9 · 10 ⁻³	-7.6 · 10 ⁻⁴ ± 1.3 · 10 ⁻⁴	-0.0025 ± 0.0005	-0.036 ± 0.008	1.3 ± 0.2	0.24 ± 0.04	0.040 ± 0.008	-0.028 ± 0.005
r		0.90	-0.62	-0.86	-0.80	-0.73	0.85	0.84	0.80	-0.82
p		6.4 · 10 ⁻⁵	0.033	2.9 · 10 ⁻⁴	0.0019	0.0067	4.3 · 10 ⁻⁴	5.4 · 10 ⁻⁴	0.0019	0.0011

*PSi: Mass calculation does not include water of hydration in opal which ranges from 6% to 10% by weight and is not well constrained.

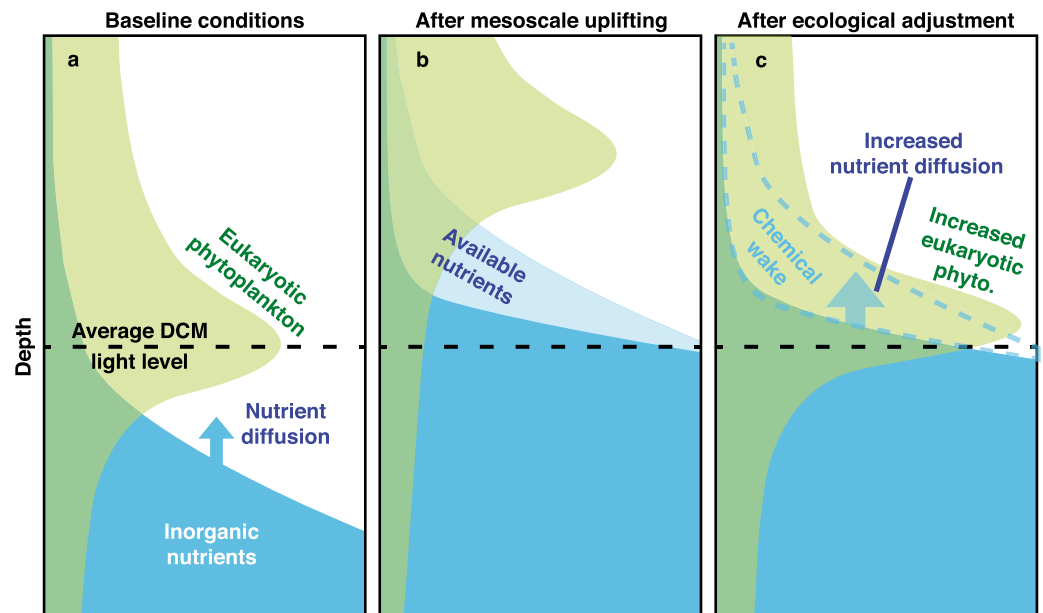


Figure 11. Ecological plankton dynamics in a mesoscale cyclone during three idealized steps: (a) Before the cyclone origin; (b) after an instantaneous uplifting caused by eddy intensification; and (c) after the ecosystem responds to the uplifting, a new deep chlorophyll maximum community emerges, and it consumes the enhanced flux of inorganic nutrients from diapycnal mixing.

range of SLA_{corr} variability observed at Station ALOHA and revealed that mesoscale motions can vertically perturb isopycnals in the lower euphotic zone by more than 100 m. These large vertical excursions alter the ambient light field on an isopycnal by more than an order of magnitude. Furthermore, we observed that light fluxes to the DCM were ~ 2 -fold greater in cyclones than in anticyclones, linking increases in available energy to increased diapycnal fluxes of nutrients. Such variations in light intensity play important roles in regulating variability in phytoplankton production in the light-limited DCM (Goldman, 1993; Goldman & McGillicuddy, 2003), with concomitant impacts on concentrations of nutrients and dissolved O_2 , a finding consistent with our analyses of historical HOT program observations.

In the current study, phytoplankton biomass remained elevated in the DCM of cyclonic eddies several weeks after the initial intensification phase (see eddy life cycles in Supplementary text S1). Based on these findings, we devised a simplified conceptual framework to describe temporal dynamics associated with cyclonic uplift of the nutricline and subsequent biological responses in the stratified ocean (Figure 11). Prior to the intensification of the cyclonic eddy, the biomass maximum of eukaryotic phytoplankton coincides with the DCM, at a depth determined by the downward light flux (Figure 11a; Letelier et al., 2004). Mesoscale uplift results in upward displacement of the DCM community and the nutricline, increasing light to otherwise light-limited phytoplankton (Figure 11b). In response to this uplift, a transient phytoplankton community utilizes the additional light energy, increasing biomass and consuming the available nutrients. Net photosynthetic production by this community fuels export of organic matter from the euphotic zone resulting in negative nutrient and positive O_2 anomalies in the waters above the DCM constituting a “chemical wake” along the displaced isopycnal surfaces (Figure 11c). An important consequence of the resulting nutrient removal is a steepening of the nutricline and presumed intensification of diapycnal nutrient fluxes, sustaining elevated eukaryotic phytoplankton biomass within the DCM (Figure 11c). Our observations indicate that, following the transient phase of nutricline erosion, light flux reaching the DCM of a cyclone can be greater than the flux reaching the DCM of an anticyclone. This finding is consistent with the ecological dynamics of the DCM layer described by Cullen (2015), whereby an increase in diapycnal nutrient flux requires a greater supply of energy (i.e., light intensity) to be consumed. Increased light accelerates the growth of phytoplankton cells in the cyclonic DCM resulting in more efficient consumption of the diapycnal nutrient flux.

In our study, we did not sample the cyclonic eddies in their intensification phase, so we do not have observations to describe the phytoplankton community responsible for the production of the chemical wake. However, the introduction of nutrient-enriched waters to the euphotic zone has been shown to promote growth of larger eukaryotic phytoplankton, which can export organic matter efficiently to the mesopelagic waters (McAndrew et al., 2007). This community would be expected to dominate phytoplankton biomass in the DCM during the transition between panels b and c in Figure 11 of our conceptual framework. As nutrients are removed, phytoplankton above the DCM, in the “chemical wake,” would be increasingly dominated by smaller cells as picoplanktonic cyanobacteria (e.g., *Prochlorococcus*), which are more typical of oligotrophic environments and whose growth and removal are more tightly balanced (McAndrew et al., 2007).

Our framework highlights understudied biogeochemical dynamics associated with the mature phase of cyclonic eddies. In contrast to previous studies (Rii et al., 2008; Sweeney et al., 2003), the novelty of our model is the focus on nutrient delivery to the lower euphotic zone attributable to diapycnal mixing in the mature stage of a cyclone rather than nutrient upwelling. Making the simplified assumption that eddy diffusivity does not vary between eddies of opposite polarity, diapycnal fluxes attributable to vertical nutrient gradients would be 9-fold and 11-fold greater for N + N and PO_4^{3-} , respectively, in the MESO-SCOPE cyclone relative to the anticyclone. Analyses of the results from a four-dimensional numerical model from Station ALOHA lend additional support to the idea that, during the mature phase of cyclonic eddies, erosion of the nutricline drives increased diapycnal nutrient fluxes supporting biomass production by eukaryotic phytoplankton near the DCM (Supplementary Text 2 and Supplementary Figure 3).

Our analyses also highlight that mesoscale dynamics can vertically decouple O_2 production from nutrient consumption. For example, during the MESO-SCOPE cruise, the 24.5 kg m^{-3} isopycnal was displaced upwards to a depth of 64 m in the center of the cyclonic eddy, which was 65 m shallower than the position of this isopycnal in the anticyclone. During the initial phase of eddy intensification, upward displacement of this isopycnal and associated increase of light in the cyclone would presumably stimulate net community production and subsequent export of this photosynthetically-derived organic matter. We see evidence of this as an excess of $23 \text{ mmol O}_2 \text{ m}^{-3}$ on the 24.5 kg m^{-3} isopycnal in the center of the cyclone relative to the average concentration of O_2 measured during the eddy survey on that isopycnal. Similarly, inorganic nutrient consumption associated with this cyclonic uplift resulted in isopycnal concentration anomalies of N + N and PO_4^{3-} of $-0.21 \text{ mmol N m}^{-3}$ and $-0.043 \text{ mmol P m}^{-3}$, respectively. The resulting $\text{O}_2:\text{N}$ and $\text{O}_2:\text{P}$ molar stoichiometries (110:1 and 535:1, respectively) suggested excess net O_2 production with respect to the net consumption of inorganic nutrients. This phenomenon was widespread in both cyclone centers, where it was observed in a depth layer above the DCM approximately between 50 and 100 m. Conversely, below 100 m, all eddy centers were characterized by a deficit in O_2 with respect to the concentration expected based on inorganic nutrient concentrations. The observation of similar variability in eddies of opposite polarity is intriguing considering the isopycnal anomalies must sum to zero across each eddy transect.

Previous studies, including several based at Station ALOHA, have reported anomalous O_2 to nutrient stoichiometries similar to those described in this study. Emerson and Hayward (1995) found that $\text{O}_2:\text{N}$ stoichiometries deviated substantially from those expected based on Redfield mineralization of organic matter in the lower euphotic zone and upper mesopelagic waters. Leveraging autonomous profiling floats equipped with O_2 and NO_3^- sensors, Johnson et al. (2010) documented consistent supersaturation of O_2 in the well-lit euphotic zone waters and an apparent deficit of NO_3^- (relative to respiratory O_2 consumption) at depth. These authors found that the “overproduction” of O_2 relative to NO_3^- consumed in the upper euphotic zone could be balanced by NO_3^- consumption without corresponding O_2 production at depth (Johnson et al., 2010). A subsequent analysis of profiling float O_2 and NO_3^- data from the subtropical North Pacific confirmed anomalous O_2 and NO_3^- stoichiometry within discrete “regimes” that differentiate based on the vertical position of isopycnal surfaces (Ascani et al., 2013).

Mechanisms proposed to explain the anomalous ratios in the concentrations of O_2 and inorganic nutrients include remineralization of C-enriched dissolved organic matter (Abell et al., 2005; Emerson & Hayward, 1995; Fawcett et al., 2018), heterotrophic bacterial assimilation of NO_3^- (Fawcett et al., 2018), phytoplankton vertical migration (Letscher & Villareal, 2018), and nitrous oxide production accompanying N oxidation (e.g., ammonia or NO_2^- oxidation; Wilson et al., 2014). Our eddy-centric observations suggest different mechanisms may produce the observed anomalies in anticyclones and cyclones. In anticyclones, the subduction of near-surface water could provide high concentrations of C-rich organic matter to the lower euphotic zone, which would be later

mineralized and result in lower O_2 concentrations relative to concentrations of inorganic nutrients that would be produced if the organic matter were mineralized in typical (i.e., Redfield) stoichiometry. Conversely, vertically-migrating phytoplankton might consume nutrients near the top of the nutricline and actively move upward to photosynthesize (Villareal et al., 1993), which could explain both the O_2 deficit below 100 m (where nutrients are taken up without O_2 production) and the O_2 surplus in the 50–100 m layer in the cyclonic eddies (where O_2 is produced without nutrient uptake).

4.2. Mesoscale Variability in Particle Fluxes

By deploying a suite of 12 individual sediment trap arrays across two adjacent eddies of opposite polarities, we obtained spatially-resolved information on particle export across a large mesoscale gradient (SLA_{corr} for these deployments ranged between -12 and 25 cm). Although export of organic matter (POC, PN, and PPO_4) was similar across and within this mesoscale gradient, total mass flux varied more than 2-fold, coincident with approximately 4-fold changes in export of PSi and PIC. Export of total mass, PSi, and PIC were all greatest in the cyclone center (lowest SLA_{corr}) and decreased linearly with increases in SLA_{corr} . Moreover, the $\delta^{15}N$ signature of sinking PN points to different sources of N supporting export across these eddies. While these observations were collected in strong mesoscale eddies, they depict several patterns of particle flux variability broadly linked with different classes of mesoscale motions, as demonstrated by the analysis of historical observations from the HOT program. Consistent with measurements in MESO-SCOPE, the HOT particle fluxes of PC, PN, and PPO_4 were not significantly correlated with SLA_{corr} , a finding previously reported by Barone et al. (2019), while a negative correlation was observed for PIC and PSi. Conversely, the increased $\delta^{15}PN$ in the MESO-SCOPE cyclone is in the opposite direction of the HOT positive correlation of $\delta^{15}PN$ and SLA_{corr} .

We believe that the mesoscale change in particle export observed in our study is not directly linked to upwelling of nutrient-rich water, but rather reflects export linked to increased diapycnal nutrient fluxes. Two pieces of evidence support this view: (a) The correlations of particle fluxes with SLA_{corr} point to a connection with the depth of the thermocline rather than with the vertical velocities that would be associated with eddy intensification or weakening; and (b) the cyclone sampled during MESO-SCOPE had its nearest intensification event 32 days before our sampling (in the Supporting Information S1). As a consequence, we attribute mesoscale variation in export detected in our measurements to the shallower and steeper nutricline associated with low SLA_{corr} , increasing nutrient supply to the lower euphotic zone and supporting abundant eukaryotic phytoplankton, including diatoms and prymnesiophytes. Subsequent export of these phytoplankton directly impacts the export of biomineralized particles. In contrast, the deeper nutricline in anticyclonic eddies appears to favor the proliferation of small picoplanktonic cyanobacteria (i.e., *Prochlorococcus*; Barone et al., 2019). The MESO-SCOPE anticyclonic eddy also contained nearly twice the concentration of dissolved iron than is typically found at the DCM at Station ALOHA, which may have supported the increase in *Prochlorococcus* abundance near the DCM (Hawco et al., 2021).

One of the most striking observations from the MESO-SCOPE sediment trap deployments were the robust inverse relationships between SLA_{corr} and PSi, PIC, and total mass flux. Enhanced PSi export has been previously reported for a wind-driven cyclone south of the Hawaiian archipelago, for a mode-water eddy in the Sargasso Sea, and for cyclones traversing Station ALOHA (Benitez-Nelson et al., 2007; Buesseler et al., 2008; Rii et al., 2008; Zhou et al., 2021); however, our observations provide evidence that cyclonic eddies may also promote PIC export. To our knowledge, these are the first observations linking export of PIC to mesoscale dynamics. The enhanced fluxes of PSi and PIC observed during MESO-SCOPE may provide some insights into the phytoplankton fueling particle export in the cyclone, specifically diatoms and prymnesiophytes, whose biomass was elevated in the DCM of the cyclone relative to the DCM of the anticyclone. Diatoms and prymnesiophytes are key phytoplankton taxa contributing to pools of PSi and PIC, respectively, but various zooplankton, including members of the Rhizaria, also have mineral skeletons composed of calcium carbonate (e.g., Foraminifera) or opal (e.g., Radiolaria). We could not quantify the abundance of large Rhizaria (>100 μm in diameter) with the methods employed in this study, so we cannot quantify contributions from these organisms to the observed variations in the export of PSi and PIC between eddies of different polarity.

A number of previous studies have identified elevated diatom and prymnesiophyte biomass in the DCM of cyclonic eddies and mode water eddies (Benitez-Nelson et al., 2007; Bidigare et al., 2003; Buesseler et al., 2008; McGillicuddy et al., 2007; Rii et al., 2008). In a microscopy-based assessment of diatoms, Scharek et al. (1999) found low contributions to sinking particle export by members of the DCM diatom assemblage, but they noted

how a substantial fraction of the diatom frustules were empty (lacking cytoplasm). Similarly, Benitez-Nelson et al. (2007) concluded that coupling between phytoplankton growth and microzooplankton grazing in Hawaiian lee cyclones resulted in export of empty diatom frustules, thereby increasing the P_{Si}: POC ratio of the trap-derived material. Based on pigment and gene-based analyses, Li et al. (2013) concluded that diatoms and prymnesiophytes comprised approximately 2% and 20%, respectively, of total chlorophyll *a* in the lower euphotic zone at Station ALOHA. However, the proportion of diatom and prymnesiophyte genes exported, relative to the euphotic zone inventory, averaged 0.15% d⁻¹ and 0.19% d⁻¹, compared to the 5% d⁻¹ P_{Si} export: inventory (Li et al., 2013). Based on high vertical resolution sampling of ²³⁴Th deficits in a mature mode water eddy in the Sargasso Sea, Buesseler et al. (2008) concluded that particle export and remineralization occur in vertically distinct regions of the upper ocean, with the waters immediately below the DCM appearing to support active particle decomposition. These results appear consistent with the interpretation that a fraction of the biomass produced by diatoms and prymnesiophytes near the DCM is mineralized before reaching the sediment traps leaving empty frustules and calcified liths, which underlie the elevated P_{Si} and PIC fluxes in the MESO-SCOPE cyclone.

In addition to clear relationships between mass, P_{Si}, and PIC fluxes, the δ¹⁵N of the exported PN demonstrated a significant inverse relationship to SLA_{corr} during MESO-SCOPE (i.e., the δ¹⁵N of PN was more enriched in the cyclone relative to the anticyclone). A number of previous studies have utilized a two-end member isotope model, leveraging differences in the δ¹⁵N signatures of deep water NO₃⁻ and N₂, to estimate the proportion of PN export supported by NO₃⁻ assimilation and N₂ fixation at Station ALOHA (Böttjer et al., 2016; Casciotti et al., 2008; Dore et al., 2002; Karl et al., 1997). Assuming only two potential sources of N (NO₃⁻ assimilation and N₂ fixation) support PN export, these observations suggest that NO₃⁻ assimilation was relatively more important in the cyclone (where NO₃⁻ appeared to support upwards of 85% of PN export) while N₂ fixation was relatively more important in the anticyclone (where N₂ fixation was estimated to support upwards of 40% of PN export). However, observations from the HOT program suggest this is not a generalized pattern for these waters: despite increased steepness in the nutricline with decreases in SLA_{corr}, the HOT observations indicate that the δ¹⁵N signature of sinking particles was positively related to variations in SLA_{corr}, opposite in sign to the variations observed during MESO-SCOPE.

To compare the magnitude of particle export to the supply of nutrients from turbulent mixing, we computed diapycnal nutrient fluxes across the top of the nutricline for the MESO-SCOPE eddies. Doing so required assuming a value for eddy diffusivity. For this purpose, we used $1.1 \times 10^{-5} \text{ m}^2 \text{ s}^{-1}$, a value determined based on a tracer release experiment conducted in the pycnocline of the North Atlantic (Ledwell et al., 1993), which is similar to the diffusivity of $10^{-5} \text{ m}^2 \text{ s}^{-1}$ that Klymak et al. (2006) estimated from the rate of dissipation of kinetic energy in the open ocean far from the Hawaiian Ridge. A tracer release experiment in the North Atlantic targeted a layer near the DCM to estimate eddy diffusivity in relation to nutrient fluxes (Ledwell et al., 2008), deriving a value for eddy diffusivity of $3.5 \times 10^{-5} \text{ m}^2 \text{ s}^{-1}$. However, the authors of this study acknowledge this value is likely elevated due to the passage of a series of storms through the sampling region (Ledwell et al., 2008); hence, we considered this diffusivity too high to be representative of the eddies sampled during the MESO-SCOPE cruise.

By assuming a diapycnal eddy diffusivity of $1.1 \times 10^{-5} \text{ m}^2 \text{ s}^{-1}$, we estimate diapycnal fluxes in the MESO-SCOPE cyclone were 0.08 mmol N m⁻² d⁻¹ and 4.5 μmol P m⁻² d⁻¹, equivalent to 20% and 34% of the measured PN and PPO₄³⁻ export fluxes, respectively. If this flux was consumed in a 20 m layer around the DCM, it would account for 10%–15% of the ¹⁴C-based primary production (Hawco et al., 2021). In comparison, diapycnal fluxes in the anticyclone were 0.009 mmol N m⁻² d⁻¹, and 0.5 μmol P m⁻² d⁻¹, equivalent to 2% and 3% of the measured PN or PPO₄³⁻ export fluxes. While the magnitude of these fluxes shows that additional sources of nitrogen and phosphorus fuel the export of particles from the euphotic zone, it remains unclear why changes in diapycnal nutrient fluxes do not appear to drive changes in the export of particulate organic matter. One possible explanation is that the mesoscale variability of other unidentified sources of nitrogen and particularly phosphorus counterbalances changes in the supply of these elements through diapycnal mixing. Another possible explanation is that the new production sustained via the implied diapycnal nutrient fluxes is exported to depths deeper than our sediment trap collections through vertically migrating zooplankton. A prior study at Station ALOHA estimated that vertical fluxes mediated by diel vertical migrators were 38% and 79% of the sediment trap fluxes of N and P, respectively (Hannides et al., 2009). This mechanism could be more pronounced in cyclones, where the higher biomass of relatively large phytoplankton could be preferentially grazed by larger zooplankton species capable of diel vertical migration.

Another process that likely varied between the eddies was N_2 fixation. Abundances of *Crocospaera*, a diazotrophic cyanobacterium, were elevated in the MESO-SCOPE anticyclone (Dugenne et al., 2020). Previous studies have documented increases in N_2 fixation and N_2 -fixing microorganism biomass associated with anticyclonic eddies (Davis & McGillicuddy, 2006; Fong et al., 2008; Wilson et al., 2017). Moreover, during the warm summer months (June–October), rates of N_2 fixation at Station ALOHA often peak during periods of positive SLA_{corr} such as those associated with anticyclones (Böttjer et al., 2016; Church et al., 2009). The gradient in $\delta^{15}N$ of PN export observed across the mesoscale eddies sampled in the current study further reinforce the apparent promotion of N_2 fixation in anticyclones during the summer in this region.

Despite the lack of variability in the export of particulate organic matter across eddies of opposite polarity, the isopycnal anomalies of O_2 and nutrients observed in the cyclone reflect the prior history of enhanced export associated with isopycnal uplift. During HL4 and MESO-SCOPE, 50–200 m depth integrated O_2 concentration anomalies in the cyclone centers were 2152 $mmol O_2 m^{-2}$ and 772 $mmol O_2 m^{-2}$ (taking into account changes in solubility), respectively, suggesting excess O_2 produced in the lower euphotic zone was not accompanied by concomitant consumption of O_2 via respiration of organic matter at the top of the mesopelagic zone. Moreover, suspended PC inventories during HL4 and MESO-SCOPE appear too low to account for the formation of O_2 isopycnal anomalies. We did not measure dissolved organic carbon, but concentrations of dissolved organic N and P were lower in the cyclone than in the anticyclones (data not shown). Such findings suggest that the organic matter produced during the formation of the O_2 and nutrient anomalies had already been exported to deeper waters. As a consequence, the biogeochemical signatures associated with nutrient consumption and O_2 production remained in the euphotic zone as a “chemical wake.” Taken together, the isopycnal anomalies and sediment trap fluxes indicate that the MESO-SCOPE cruise likely sampled the cyclonic eddy at some point after the peak period of organic matter export. However, the enhanced diapycnal nutrient fluxes during the mature stage of the eddy kept sustaining a community of diatoms and prymnesiophytes in the DCM layer. Some of these cells underwent mineralization in the upper 150 m, exporting empty frustules and calcified liths that enhanced PSi and PIC fluxes.

5. Conclusions

By sampling adjacent eddies of opposite polarity we identified several impacts of mesoscale motions on plankton biology and upper ocean biogeochemistry in the subtropical North Pacific Ocean. Some key findings that emerged from our study are:

1. Phytoplankton growth following isopycnal uplift in cyclones steepened the vertical gradients in inorganic nutrients through the biological erosion of the top of the nutricline. This presumably increased the diapycnal flux of nutrients delivered to the lower euphotic zone and supported increased eukaryotic phytoplankton biomass during the mature phase of the eddies. Conversely, depression of isopycnals in anticyclones decreased nutrient concentration gradients in the lower euphotic zone, a dynamic that appeared to increase *Prochlorococcus* biomass above the DCM.
2. Mesoscale changes in inorganic nutrients and dissolved O_2 concentrations are vertically decoupled. For example, upward displacement of isopycnals associated with cyclonic eddies resulted in peak consumption of inorganic nutrients occurring deeper than the layer where O_2 production was maximal. In contrast, both cyclones and anticyclones appeared to have less O_2 than expected based on nutrient concentrations in the layer below the DCM.
3. Particle-associated biomineral fluxes of PSi and PIC were inversely related to SLA_{corr} despite no differences in export of POC, PN, and PPO_4^{3-} . Elevated biomineral export at low SLA_{corr} presumably reflects increased contributions from silicifying and calcifying plankton consistent with observations of elevated biomass of Bacillariophyceae and Prymnesiophytes in the cyclone DCM. Moreover, the $\delta^{15}N$ of sinking particles revealed differences in N sources supporting production across adjacent eddies, with a larger contribution by N_2 fixation in the anticyclone.

Our study highlights the spatiotemporal complexity of ocean ecosystems, and the inherent challenges such complexity presents to Eulerian observations such as the HOT program. Across a region of the ocean stretching a few hundreds of kilometers, the presence of strong, mature, mesoscale eddies of opposite polarity resulted in striking differences in ocean biogeochemistry. We found eddy-dependent isopycnal displacements through the upper ocean light field alter the steepness of the nutricline, influence the biomass of eukaryotic phytoplankton

(including members of the prymnesiophytes and diatoms) and *Prochlorococcus*, and impact the export of opal and carbonate. These observations expand our understanding of the biogeochemical impacts of mesoscale motions by describing the stoichiometry of the erosion of the nutricline in cyclonic eddies and by highlighting a series of cascading dynamics that result from this erosion.

Data Availability Statement

Sea level anomaly is available from the Copernicus Marine and Environment Monitoring Service (<http://marine.copernicus.eu>). Hawaii Ocean Time-series observations are available through HOT-DOGS (<http://hahana.soest.hawaii.edu/hot/hot-dogs/>). Results from the numerical model can be accessed at <https://doi.org/10.6075/JOBR8QJ1>. The altimetric Mesoscale Eddy Trajectories Atlas (META2.0) was produced by SSALTO/DUACS and distributed by AVISO+ (<https://aviso.altimetry.fr>) with support from CNES, in collaboration with Oregon State University with support from NASA. All other measurements used for the analyses of this manuscript are available at <https://doi.org/10.5281/zenodo.5048504>.

Acknowledgments

We warmly thank Tara Clemente (University of Hawaii) for her leadership during the HOE-Legacy 4 and MESO-SCOPE expeditions. We are also grateful to Tim Burrell, Eric Shimabukuro, and Ryan Tabata (University of Hawaii) for their tireless efforts during field operations. We are grateful to Joshua Weitz and David Demory (Georgia Institute of Technology) for their thoughtful comments on the manuscript. We thank Susan Curless, Eric Grabowski, and Alexa Nelson (University of Hawaii) for the analysis of inorganic nutrients and sinking particle fluxes. The isotopic composition of nitrogen of sinking particles was measured by the Biogeochemical Stable Isotope Facility (University of Hawaii). This work was supported by grants from the Simons Foundation (#329108 to DMK, EFD, MJF, MJC, AEW, SGJ; 721252 to DMK; 721223 to EFD; 721221 to MJC; 721256 to AEW; 721250 to SGJ).

References

- Abell, J., Emerson, S., & Keil, R. G. (2005). Using preformed nitrate to infer decadal changes in DOM remineralization in the subtropical North Pacific. *Global Biogeochemical Cycles*, *19*(1). <https://doi.org/10.1029/2004GB002285>
- Anderson, G. C. (1969). Subsurface chlorophyll maximum in the northeast Pacific Ocean. *Limnology & Oceanography*, *14*, 386–391. <https://doi.org/10.4319/lo.1969.14.3.0386>
- Anderson, L. A. (1995). On the hydrogen and oxygen content of marine phytoplankton. *Deep-Sea Research Part I Oceanographic Research Papers*, *42*, 1675–1680. [https://doi.org/10.1016/0967-0637\(95\)00072-E](https://doi.org/10.1016/0967-0637(95)00072-E)
- Anderson, L. A., & Sarmiento, J. L. (1994). Redfield ratios of remineralization determined by nutrient data analysis. *Global Biogeochemical Cycles*, *8*(1), 65–80. <https://doi.org/10.1029/93GB03318>
- Ascani, F., Richards, K. J., Firing, E., Grant, S., Johnson, K. S., Jia, Y., & Karl, D. M. (2013). Physical and biological controls of nitrate concentrations in the upper subtropical North Pacific Ocean. *Deep-Sea Research Part II: Topical Studies in Oceanography*, *93*, 119–134. <https://doi.org/10.1016/j.dsr2.2013.01.034>
- Bahamón, N., Velasquez, Z., & Cruzado, A. (2003). Chlorophyll a and nitrogen flux in the tropical North Atlantic Ocean. *Deep-Sea Research Part I: Oceanographic Research Papers*, *50*(10–11), 1189–1203. [https://doi.org/10.1016/S0967-0637\(03\)00145-6](https://doi.org/10.1016/S0967-0637(03)00145-6)
- Barone, B., Coenen, A. R., Beckett, S. J., McGillicuddy, D. J., Weitz, J. S., & Karl, D. M. (2019). The ecological and biogeochemical state of the North Pacific Subtropical Gyre is linked to sea surface height. *Journal of Marine Research*, *77*(2), 215–245. <https://doi.org/10.1357/002224019828474241>
- Benitez-Nelson, C. R., Bidigare, R. R., Dickey, T. D., Landry, M. R., Leonard, C. L., Brown, S. L., & Yang, E. J. (2007). Mesoscale eddies drive increased silica export in the subtropical Pacific Ocean. *Science*, *316*(5827), 1017–1021. <https://doi.org/10.1126/science.1136221>
- Bidigare, R. R., Benitez-Nelson, C., Leonard, C. L., Quay, P. D., Parsons, M. L., Foley, D. G., & Seki, M. P. (2003). Influence of a cyclonic eddy on microheterotroph biomass and carbon export in the lee of Hawaii. *Geophysical Research Letters*, *30*(6). <https://doi.org/10.1029/2002GL016393>
- Böttjer, D., Dore, J. E., Karl, D. M., Letelier, R. M., Mahaffey, C., Wilson, S. T., et al. (2016). Temporal variability of nitrogen fixation and particulate nitrogen export at Station ALOHA. *Limnology & Oceanography*, *62*(1), 200–216. <https://doi.org/10.1002/lno.10386>
- Brzezinski, M. A., & Nelson, D. M. (1989). Seasonal changes in the silicon cycle within a Gulf Stream warm-core ring. *Deep-Sea Research Part A: Oceanographic Research Papers*, *36*(7), 1009–1030. [https://doi.org/10.1016/0198-0149\(89\)90075-7](https://doi.org/10.1016/0198-0149(89)90075-7)
- Buesseler, K. O., Lamborg, C., Cai, P., Escoube, R., Johnson, R., Pike, S., & Verdeny, E. (2008). Particle fluxes associated with mesoscale eddies in the Sargasso Sea. *Deep-Sea Research Part II: Topical Studies in Oceanography*, *55*(10–13), 1426–1444. <https://doi.org/10.1016/j.dsr2.2008.02.007>
- Carpenter, J. H. (1965). The accuracy of the Winkler method for dissolved oxygen analysis. *Limnology & Oceanography*, *10*(1), 135–140. <https://doi.org/10.4319/lo.1965.10.1.0135>
- Casciotti, K. L., Trull, T. W., Glover, D. M., & Davies, D. (2008). Constraints on nitrogen cycling at the subtropical North Pacific station ALOHA from isotopic measurements of nitrate and particulate nitrogen. *Deep-Sea Research Part II: Topical Studies in Oceanography*, *55*(14–15), 1661–1672. <https://doi.org/10.1016/j.dsr2.2008.04.017>
- Chelton, D. B., Gaube, P., Schlax, M. G., Early, J. J., & Samelson, R. M. (2011). The influence of nonlinear mesoscale eddies on near-surface oceanic chlorophyll. *Science*, *334*, 328–332. <https://doi.org/10.1126/science.1208897>
- Chelton, D. B., Schlax, M. G., Samelson, R. M., & de Szoeke, R. A. (2007). Global observations of large oceanic eddies. *Geophysical Research Letters*, *34*(15). <https://doi.org/10.1029/2007GL030812>
- Church, M. J., Mahaffey, C., Letelier, R. M., Lukas, R., Zehr, J. P., & Karl, D. M. (2009). Physical forcing of nitrogen fixation and diazotroph community structure in the North Pacific subtropical gyre. *Global Biogeochemical Cycles*, *23*. <https://doi.org/10.1029/2008GB003418>
- Cullen, J. J. (2015). Subsurface chlorophyll maximum layers: Enduring enigma or mystery solved? *Annual Review of Marine Science*, *7*, 207–239. <https://doi.org/10.1146/annurev-marine-010213-135111>
- Cullen, J. J., & Eppley, R. W. (1981). Chlorophyll maximum layers of the Southern California Bight and possible mechanisms of their formation and maintenance. *Oceanologica Acta*, *4*(1), 23–32.
- Davis, C. S., & McGillicuddy, D. J. (2006). Transatlantic abundance of the N₂-fixing colonial cyanobacterium *Trichodesmium*. *Science*, *312*(5779), 1517–1520. <https://doi.org/10.1126/science.1123570>
- Dore, J. E., Brum, J. R., Tupas, L. M., & Karl, D. M. (2002). Seasonal and interannual variability in sources of nitrogen supporting export in the oligotrophic subtropical North Pacific Ocean. *Limnology & Oceanography*, *47*(6), 1595–1607. <https://doi.org/10.4319/lo.2002.47.6.1595>
- Dore, J. E., Houlihan, T., Hebel, D. V., Tien, G., Tupas, L., & Karl, D. M. (1996). Freezing as a method of sample preservation for the analysis of dissolved inorganic nutrients in seawater. *Marine Chemistry*, *54*(1), 53. [https://doi.org/10.1016/0304-4203\(96\)00004-7](https://doi.org/10.1016/0304-4203(96)00004-7)

- Dugenne, M., Henderikx Freitas, F., Wilson, S. T., Karl, D. M., & White, A. E. (2020). Life and death of *Crocospaera* sp. in the Pacific Ocean: Fine scale predator–prey dynamics. *Limnology & Oceanography*, *65*, 2603–2617. <https://doi.org/10.1002/lno.11473>
- Emerson, S., & Hayward, T. L. (1995). Chemical tracers of biological processes in shallow waters of North Pacific: Preformed nitrate distributions. *Journal of Marine Research*, *53*(3), 499–513. <https://doi.org/10.1357/0022240953213179>
- Falkowski, P. G., Ziemann, D., Kolber, Z., & Bienfang, P. K. (1991). Role of eddy pumping in enhancing primary production in the ocean. *Nature*, *352*(6330), 55–58. <https://doi.org/10.1038/352055a0>
- Fawcett, S. E., Johnson, K. S., Riser, S. C., Van Oostende, N., & Sigman, D. M. (2018). Low-nutrient organic matter in the Sargasso Sea thermocline: A hypothesis for its role, identity, and carbon cycle implications. *Marine Chemistry*, *207*, 108–123. <https://doi.org/10.1016/j.marchem.2018.10.008>
- Fong, A. A., Karl, D. M., Lukas, R., Letelier, R. M., Zehr, J. P., & Church, M. J. (2008). Nitrogen fixation in an anticyclonic eddy in the oligotrophic North Pacific Ocean. *The ISME Journal*, *2*(6), 663–676. <https://doi.org/10.1038/ismej.2008.22>
- Foreman, R. K., Segura-Noguera, M., & Karl, D. M. (2016). Validation of Ti(III) as a reducing agent in the chemiluminescent determination of nitrate and nitrite in seawater. *Marine Chemistry*, *186*, 83–89. <https://doi.org/10.1016/j.marchem.2016.08.003>
- Gaube, P., McGillicuddy, D. J., Chelton, D. B., Behrenfeld, M. J., & Strutton, P. G. (2014). Regional variations in the influence of mesoscale eddies on near-surface chlorophyll. *Journal of Geophysical Research: Oceans*, *119*, 8195–8220. <https://doi.org/10.1002/2014JC010111>
- Goldman, J. C. (1993). Potential role of large oceanic diatoms in new primary production. *Deep-Sea Research Part I: Oceanographic Research Papers*, *40*(1), 159–168. [https://doi.org/10.1016/0967-0637\(93\)90059-C](https://doi.org/10.1016/0967-0637(93)90059-C)
- Goldman, J. C., & McGillicuddy, D. J., Jr. (2003). Effect of large marine diatoms growing at low light on episodic new production. *Limnology & Oceanography*, *48*, 1176–1182. <https://doi.org/10.4319/lo.2003.48.3.1176>
- Gordon, H. R., & McCluney, W. R. (1975). Estimation of the depth of sunlight penetration in the sea for remote sensing. *Applied Optics*, *14*(2), 413–416. <https://doi.org/10.1364/AO.14.000413>
- Grabowski, E., Letelier, R. M., Laws, E. A., & Karl, D. M. (2019). Coupling carbon and energy fluxes in the North Pacific Subtropical Gyre. *Nature Communications*, *10*(1), 1–9. <https://doi.org/10.1038/s41467-019-09772-z>
- Guo, M., Xiu, P., Chai, F., & Xue, H. (2019). Mesoscale and submesoscale contributions to high sea surface chlorophyll in subtropical gyres. *Geophysical Research Letters*, *46*(22), 13217–13226. <https://doi.org/10.1029/2019GL085278>
- Hannides, C. C., Landry, M. R., Benitez-Nelson, C. R., Styles, R. M., Montoya, J. P., & Karl, D. M. (2009). Export stoichiometry and migrant-mediated flux of phosphorus in the North Pacific Subtropical Gyre. *Deep-Sea Research Part I: Oceanographic Research Papers*, *56*(1), 73–88. <https://doi.org/10.1016/j.dsr.2008.08.003>
- Hawco, N. J., Barone, B., Church, M. J., Babcock-Adams, L., Repeta, D. J., Wear, E. K., et al. (2021). Iron depletion in the deep chlorophyll maximum: Mesoscale eddies as natural iron fertilization experiments. *Global Biogeochemical Cycles*, *35*(12), e2021GB007112. <https://doi.org/10.1029/2021GB007112>
- Herbland, A., & Voituriez, B. (1979). Hydrological structure analysis for estimating the primary production in the tropical Atlantic Ocean. *Journal of Marine Research*, *37*(1), 87–101.
- Johnson, K. S., Riser, S. C., & Karl, D. M. (2010). Nitrate supply from deep to near-surface waters of the North Pacific subtropical gyre. *Nature*, *465*(7301), 1062–1065. <https://doi.org/10.1038/nature09170>
- Karl, D., Letelier, R., Tupas, L., Dore, J., Christian, J., & Hebel, D. (1997). The role of nitrogen fixation in biogeochemical cycling in the subtropical North Pacific Ocean. *Nature*, *388*(6642), 533–538. <https://doi.org/10.1038/41474>
- Karl, D. M. (1999). A sea of change: Biogeochemical variability in the North Pacific Subtropical Gyre. *Ecosystems*, *2*(3), 181–214. <https://doi.org/10.1007/s100219900068>
- Karl, D. M., Bidigare, R. R., & Letelier, R. M. (2001). Long-term changes in plankton community structure and productivity in the North Pacific Subtropical Gyre: The domain shift hypothesis. *Deep-Sea Research Part II: Topical Studies in Oceanography*, *48*, 1449–1470. [https://doi.org/10.1016/S0967-0645\(00\)00149-1](https://doi.org/10.1016/S0967-0645(00)00149-1)
- Karl, D. M., Björkman, K. M., Dore, J. E., Fujieki, L., Hebel, D. V., Houlihan, T., & Tupas, L. M. (2001). Ecological nitrogen-to-phosphorus stoichiometry at station ALOHA. *Deep-Sea Research Part II: Topical Studies in Oceanography*, *48*, 1529–1566. [https://doi.org/10.1016/S0967-0645\(00\)00152-1](https://doi.org/10.1016/S0967-0645(00)00152-1)
- Karl, D. M., Christian, J. R., Dore, J. E., Hebel, D. V., Letelier, R. M., Tupas, L. M., & Winn, C. D. (1996). Seasonal and interannual variability in primary production and particle flux at Station ALOHA. *Deep-Sea Research Part II: Topical Studies in Oceanography*, *43*(2–3), 539–568. [https://doi.org/10.1016/0967-0645\(96\)00002-1](https://doi.org/10.1016/0967-0645(96)00002-1)
- Karl, D. M., & Lukas, R. (1996). The Hawaii Ocean time-series (HOT) program: Background, rationale and field implementation. *Deep-Sea Research Part II: Topical Studies in Oceanography*, *43*(2–3), 129–156. [https://doi.org/10.1016/0967-0645\(96\)00005-7](https://doi.org/10.1016/0967-0645(96)00005-7)
- Klymak, J. M., Moum, J. N., Nash, J. D., Kunze, E., Girton, J. B., Carter, G. S., & Gregg, M. C. (2006). An estimate of tidal energy lost to turbulence at the Hawaiian Ridge. *Journal of Physical Oceanography*, *36*(6), 1148–1164. <https://doi.org/10.1175/JPO2885.1>
- Knauer, G. A., Martin, J. H., & Bruland, K. W. (1979). Fluxes of particulate carbon, nitrogen, and phosphorus in the upper water column of the northeast Pacific. *Deep-Sea Research Part A: Oceanographic Research Papers*, *26*(1), 97–108. [https://doi.org/10.1016/0198-0149\(79\)90089-X](https://doi.org/10.1016/0198-0149(79)90089-X)
- Kuwahara, V. S., Nencioli, F., Dickey, T. D., Rii, Y. M., & Bidigare, R. R. (2008). Physical dynamics and biological implications of cyclone Noah in the lee of Hawai'i during E-Flux I. *Deep-Sea Research Part II: Topical Studies in Oceanography*, *55*, 1231–1251. <https://doi.org/10.1016/j.dsr2.2008.01.007>
- Ledwell, J. R., McGillicuddy, D. J., Jr., & Anderson, L. A. (2008). Nutrient flux into an intense deep chlorophyll layer in a mode-water eddy. *Deep-Sea Research Part II: Topical Studies in Oceanography*, *55*(10–13), 1139–1160. <https://doi.org/10.1016/j.dsr2.2008.02.005>
- Ledwell, J. R., Watson, A. J., & Law, C. S. (1993). Evidence for slow mixing across the pycnocline from an open-ocean tracer-release experiment. *Nature*, *364*(6439), 701–703. <https://doi.org/10.1038/364701a0>
- Letelier, R. M., Karl, D. M., Abbott, M. R., & Bidigare, R. R. (2004). Light driven seasonal patterns of chlorophyll and nitrate in the lower euphotic zone of the North Pacific Subtropical Gyre. *Limnology & Oceanography*, *49*, 508–519. <https://doi.org/10.4319/lo.2004.49.2.0508>
- Letelier, R. M., Karl, D. M., Abbott, M. R., Flament, P., Freilich, M., Lukas, R., & Strub, T. (2000). Role of late winter mesoscale events in the biogeochemical variability of the upper water column of the North Pacific Subtropical Gyre. *Journal of Geophysical Research*, *105*, 28723–28739. <https://doi.org/10.1029/1999JC000306>
- Letscher, R. T., & Villareal, T. A. (2018). Evaluation of the seasonal formation of subsurface negative preformed nitrate anomalies in the subtropical North Pacific and North Atlantic. *Biogeosciences*, *15*(21), 6461–6480. <https://doi.org/10.5194/bg-15-6461-2018>
- Lewis, M. R., Hebert, D., Harrison, W. G., Platt, T., & Oakey, N. S. (1986). Vertical nitrate fluxes in the oligotrophic ocean. *Science*, *234*(4778), 870–873. <https://doi.org/10.1126/science.234.4778.870>
- Li, B., Karl, D. M., Letelier, R. M., Bidigare, R. R., & Church, M. J. (2013). Variability of chromophytic phytoplankton in the North Pacific Subtropical Gyre. *Deep-Sea Research Part II: Topical Studies in Oceanography*, *93*, 84–95. <https://doi.org/10.1016/j.dsr2.2013.03.007>

- Li, B., Karl, D. M., Letelier, R. M., & Church, M. J. (2011). Size-dependent photosynthetic variability in the North Pacific Subtropical Gyre. *Marine Ecology Progress Series*, 440, 27–40. <https://doi.org/10.3354/meps09345>
- Mackas, D. L., Denman, K. L., & Abbott, M. R. (1985). Plankton patchiness: Biology in the physical vernacular. *Bulletin of Marine Science*, 37(2), 652–674.
- Malmstrom, R. R., Coe, A., Kettler, G. C., Martiny, A. C., Frias-Lopez, J., Zinser, E. R., & Chisholm, S. W. (2010). Temporal dynamics of *Prochlorococcus* ecotypes in the Atlantic and Pacific oceans. *The ISME Journal*, 4, 1252–1264. <https://doi.org/10.1038/ismej.2010.60>
- McAndrew, P. M., Björkman, K. M., Church, M. J., Morris, P. J., Jachowski, N., Williams, P. J. L. B., & Karl, D. M. (2007). Metabolic response of oligotrophic plankton communities to deep water nutrient enrichment. *Marine Ecology Progress Series*, 332, 63–75. <https://doi.org/10.3354/meps332063>
- McClain, C. R., Signorini, S. R., & Christian, J. R. (2004). Subtropical gyre variability observed by ocean-color satellites. *Deep-Sea Research Part II: Topical Studies in Oceanography*, 51(1–3), 281–301. <https://doi.org/10.1016/j.dsr2.2003.08.002>
- McGillicuddy, D. J., Jr, Anderson, L. A., Bates, N. R., Bibby, T., Buesseler, K. O., Carlson, C. A., & Steinberg, D. K. (2007). Eddy/wind interactions stimulate extraordinary mid-ocean plankton blooms. *Science*, 316(5827), 1021–1026. <https://doi.org/10.1126/science.1136256>
- McGillicuddy, D. J., Jr, Johnson, R. J., Siegel, D. A., Michaels, A. F., Bates, N., & Knap, A. H. (1999). Mesoscale variations of biogeochemical properties in the Sargasso Sea. *Journal of Geophysical Research*, 104, 13381–13394. <https://doi.org/10.1029/1999JC900021>
- McGillicuddy, D. J., Jr, & Robinson, A. R. (1997). Eddy-induced nutrient supply and new production in the Sargasso Sea. *Deep-Sea Research Part I: Oceanographic Research Papers*, 44, 1427–1450. [https://doi.org/10.1016/S0967-0637\(97\)00024-1](https://doi.org/10.1016/S0967-0637(97)00024-1)
- Menden-Deuer, S., & Lessard, E. J. (2000). Carbon to volume relationships for dinoflagellates, diatoms, and other protist plankton. *Limnology & Oceanography*, 45, 569–579. <https://doi.org/10.4319/lo.2000.45.3.0569>
- Munk, W. (2002). The evolution of physical oceanography in the last hundred years. *Oceanography*, 15(1), 135–142. <https://doi.org/10.5670/oceanog.2002.45>
- Pedlosky, J. (1990). The dynamics of the oceanic subtropical gyres. *Science*, 248(4953), 316–322. <https://doi.org/10.1126/science.248.4953.316>
- Redfield, A. C. (1958). The biological control of chemical factors in the environment. *American Scientist*, 46(3), 205–222.
- Rii, Y. M., Brown, S. L., Nencioli, F., Kuwahara, V., Dickey, T., Karl, D. M., & Bidigare, R. R. (2008). The transient oasis: Nutrient-phytoplankton dynamics and particle export in Hawaiian lee cyclones. *Deep-Sea Research Part II: Topical Studies in Oceanography*, 55(10–13), 1275–1290. <https://doi.org/10.1016/j.dsr2.2008.01.013>
- Roesler, C., Uitz, J., Claustre, H., Boss, E., Xing, X., Organelli, E., & Barbiereux, M. (2017). Recommendations for obtaining unbiased chlorophyll estimates from in situ chlorophyll fluorometers: A global analysis of WET Labs ECO sensors. *Limnology and Oceanography: Methods*, 15(6), 572–585. <https://doi.org/10.1002/lom3.10185>
- Scharek, R., Latasa, M., Karl, D. M., & Bidigare, R. R. (1999). Temporal variations in diatom abundance and downward vertical flux in the oligotrophic North Pacific gyre. *Deep-Sea Research Part I: Oceanographic Research Papers*, 46(6), 1051–1075. [https://doi.org/10.1016/S0967-0637\(98\)00102-2](https://doi.org/10.1016/S0967-0637(98)00102-2)
- Schlax, M. G., & Chelton, D. B. (2016). *The “growing method” of eddy identification and tracking in two and three dimensions*. College of Earth, Ocean and Atmospheric Sciences, Oregon State University.
- Sosik, H. M., & Olson, R. J. (2007). Automated taxonomic classification of phytoplankton sampled with imaging in flow cytometry. *Limnology and Oceanography: Methods*, 5, 204–216. <https://doi.org/10.4319/lom.2007.5.204>
- Strickland, J. D. H., & Parsons, T. R. (1972). *A practical handbook of seawater analysis* (2nd ed.). Fisheries Research Board of Canada.
- Sweeney, E. N., McGillicuddy, D. J., Jr, & Buesseler, K. O. (2003). Biogeochemical impacts due to mesoscale eddy activity in the Sargasso Sea as measured at the Bermuda Atlantic Time-series Study (BATS). *Deep-Sea Research Part II: Topical Studies in Oceanography*, 50(22–26), 3017–3039. <https://doi.org/10.1016/j.dsr2.2003.07.008>
- Vaillancourt, R. D., Marra, J., Seki, M. P., Parsons, M. L., & Bidigare, R. R. (2003). Impact of a cyclonic eddy on phytoplankton community structure and phytoplankton competency in the subtropical North Pacific Ocean. *Deep-Sea Research Part I: Oceanographic Research Papers*, 50, 829–847. [https://doi.org/10.1016/S0967-0637\(03\)00059-1](https://doi.org/10.1016/S0967-0637(03)00059-1)
- Venrick, E. L. (1982). Phytoplankton in an oligotrophic ocean: Observations and questions. *Ecological Monographs*, 52, 129–154. <https://doi.org/10.2307/1942608>
- Venrick, E. L. (1990). Mesoscale patterns of chlorophyll *a* in the central North Pacific. *Deep-Sea Research Part A: Oceanographic Research Papers*, 37(6), 1017–1031. [https://doi.org/10.1016/0198-0149\(90\)90108-8](https://doi.org/10.1016/0198-0149(90)90108-8)
- Venrick, E. L. (1999). Phytoplankton species structure in the central North Pacific 1973–1996: Variability and persistence. *Journal of Plankton Research*, 21, 1029–1042. <https://doi.org/10.1093/plankt/21.6.1029>
- Villareal, T., Altabet, M., & Culver-Rymsza, K. (1993). Nitrogen transport by vertically migrating diatom mats in the North Pacific Ocean. *Nature*, 363, 709–712. <https://doi.org/10.1038/363709a0>
- Wilson, S. T., Aylward, F. O., Ribalet, F., Barone, B., Casey, J. R., Connell, P. E., et al. (2017). Coordinated regulation of growth, activity and transcription in natural populations of the unicellular nitrogen-fixing cyanobacterium *Crocospaera*. *Nature Microbiology*, 2(9), 1–9. <https://doi.org/10.1038/nmicrobiol.2017.118>
- Wilson, S. T., del Valle, D., Segura-Noguera, M., & Karl, D. (2014). A role for nitrite in the production of nitrous oxide in the lower euphotic zone of the oligotrophic North Pacific Ocean. *Deep-Sea Research Part I: Oceanographic Research Papers*, 85, 47–55. <https://doi.org/10.1016/j.dsr.2013.11.008>
- Wunsch, C. (1997). The vertical partition of oceanic horizontal kinetic energy. *Journal of Physical Oceanography*, 27, 1770–1794. [https://doi.org/10.1175/1520-0485\(1997\)027<1770:tvpooh>2.0.co;2](https://doi.org/10.1175/1520-0485(1997)027<1770:tvpooh>2.0.co;2)
- Zhou, K., Benitez-Nelson, C. R., Huang, J., Xiu, P., Sun, Z., & Dai, M. (2021). Cyclonic eddies modulate temporal and spatial decoupling of particulate carbon, nitrogen, and biogenic silica export in the North Pacific Subtropical Gyre. *Limnology & Oceanography*, 66(9), 3508–3522. <https://doi.org/10.1002/lno.11895>

References From the Supporting Information

- Dutkiewicz, S., Hickman, A. E., Jahn, O., Gregg, W. W., Mouw, C. B., & Follows, M. J. (2015). Capturing optically important constituents and properties in a marine biogeochemical and ecosystem model. *Biogeosciences*, 12, 4447–4481. <https://doi.org/10.5194/bg-12-4447-2015>
- Marshall, J., Hill, C., Perelman, L., & Adcroft, A. (1997). Hydrostatic, quasi-hydrostatic, and nonhydrostatic ocean modeling. *Journal of Geophysical Research*, 102, 5733–5752. <https://doi.org/10.1029/96JC02776>
- Menemenlis, D., Campin, J. M., Heimbach, P., Hill, C., Lee, T., Nguyen, A., & Zhang, H. (2008). ECCO2: High resolution global ocean and sea ice data synthesis. *Mercator Ocean Quarterly Newsletter*, 31, 13–21.